Chapter 2: Crystallographic characterisation of the dynamic motion exhibited by as-synthesised $(Me_2NH_2)[In(ABDC)_2]$ during solvent removal (ABDC = 2-aminobenzene-1,4-dicarboxylate)

2.1 Abstract

The previously unobserved flexible behaviour exhibited by indium carboxylate MOF $(Me_2NH_2)[In(ABDC)_2]$ is presented using a combination of *in situ* and *ex situ* crystallographic heating experiments. The two dimensional flexibility occurs upon both removal and gain of guest molecules, and strongly affects the accessible porosity of the material. The dynamics of the system occurs in a rare continuous process, while maintaining its integrity as a single crystal, allowing accurate structural characterisation.

2.2 Introduction

The previous chapter reported on the wide range of dynamic motions exhibited by a class of porous inorganic coordination polymers known as metal-organic frameworks (MOFs). These dynamic responses are usually caused by a removal, or a change, of the contained guest molecules. The removal of the guests is often required before use in potential applications, and therefore understanding the framework responses are of substantial significance. In particular chapter 1 highlighted the need to develop and understand MOFs exhibiting continuous flexibility, a field currently poorly represented in the scientific literature. The work in this chapter addresses this goal, focusing on indium carboxylate framework $(Me_2NH_2)[In(ABDC)_2]$. A previous report on this MOF, which described the crystal structure, the solvent removal via $CHCl_3$ exchange, and the gas adsorption properties, demonstrated an excellent selectivity between CO_2 and CH_4 uptake in a framework which appeared to possess a rigid structure.[1] This chapter and subsequent chapters however present a detailed analysis of the MOF, and demonstrate that it exhibits extensive dynamic behaviour of a rare continuous breathing type.

The MOF is constructed from In(III) centres coordinated by four chelating 2-aminobenzene-1,4-dicarboxylate (ABDC or 2-aminoterephthalate) ligands in a flattened tetrahedral geometry. The ditopic benzene-1,4-dicarboxylate ligands connect to other indium centres resulting in a 3D diamondoid network that is doubly interpenetrated. The negative charge of the framework is balanced by one $Me_2NH_2^+$ cation per indium centre, which is formed from decomposition of the DMF

solvent during the solvothermal synthesis. The crystallographic characterisation from the original publication[1] showed that the amino group displayed only one location within the asymmetric unit, and did not exhibit the typical site disorder around the aromatic ring common in other MOFs containing the 2-aminoterephthalate ligand.[2–7] Only the anionic framework was modelled in the original publication and the disordered cations and solvent molecules contained within the pore space were accounted for by using the SQUEEZE[8] routine of the program PLATON.[9] The basic building unit and the two symmetry-equivalent interpenetrated networks can be seen in Figure 1 a) and b) respectively.

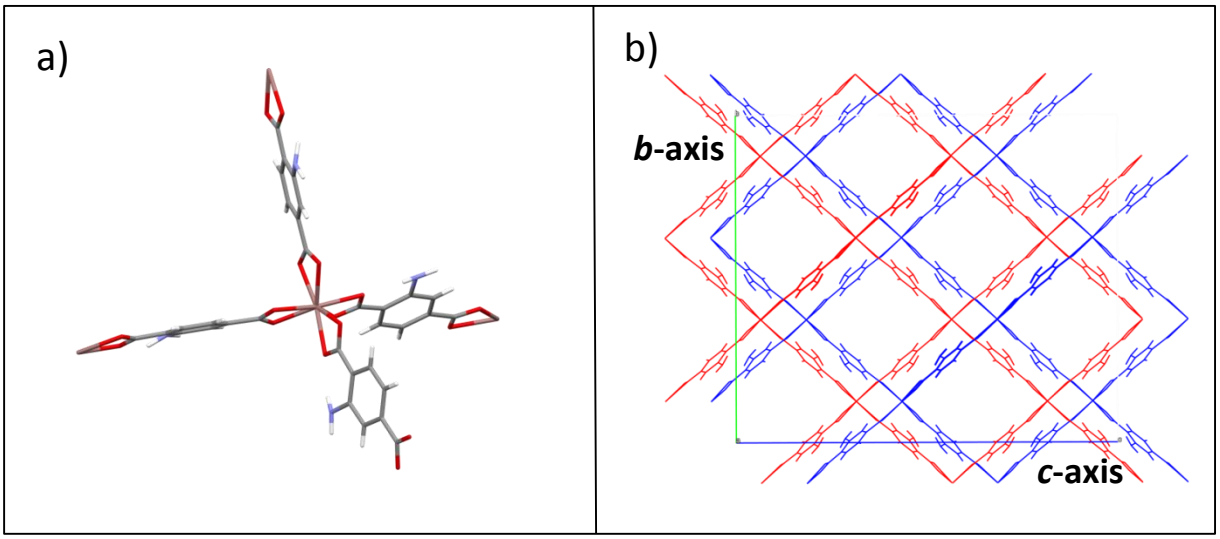

Figure 1 - Capped Stick representation of the framework $[In(ABDC)_2]^-$ from the MOF $(Me_2NH_2)[In(ABDC)_2]$.[1] a) The eight-coordinate indium centre surrounded by four 2-aminoterethalate ligands; b) view down the *a*-axis looking at the two extended networks, shown in red and blue.

The framework exhibits reasonable porosity, displaying one-dimensional channels running parallel to *a*-axis. The pores contain both the charge-balancing cations and guest DMF solvent molecules from the synthesis. One of these channels is displayed in Figure 2 with the pore highlighted in blue.

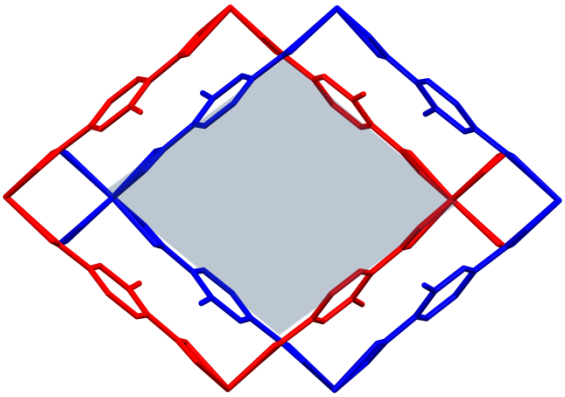

Figure 2 - Section of framework from the crystal structure of $(Me_2NH_2)[In(ABDC)_2]$ viewed down the *a*-axis showing a single pore and illustrating its diamond shape

The diamond-shaped channel in Figures 1 and 2 is viewed down the *a*-axis, with the *b*-axis vertical and the *c*-axis horizontal. This view will be used consistently throughout the chapter. These channels are defined by two intertwined helical motifs displayed in Figure 3, which views the MOF down the *c*-axis, orthogonal to the view in Figure 2. The pore space Figure 3 has also been highlighted in blue for clarity.

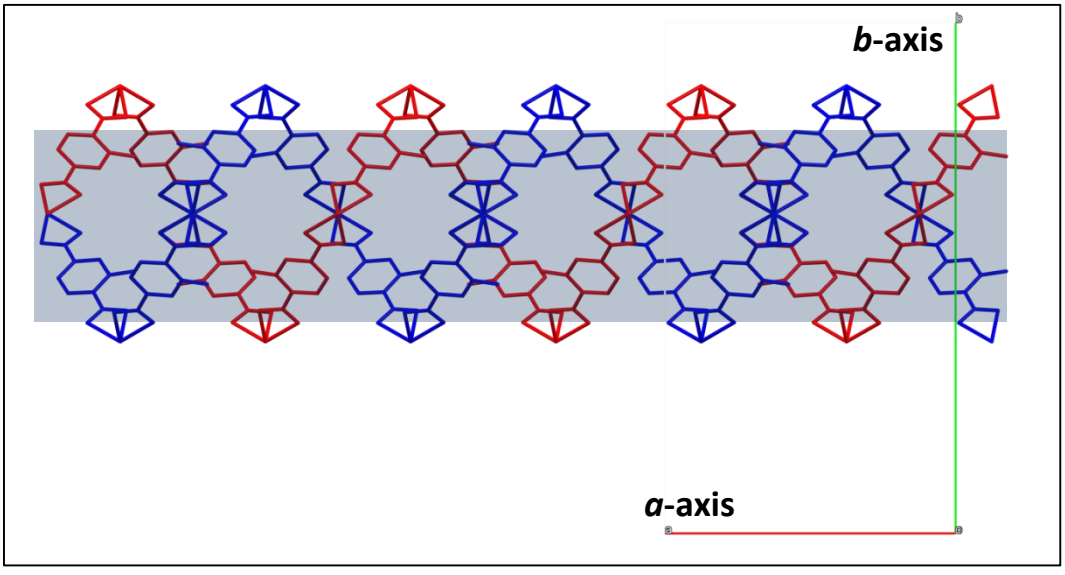

Figure 3 - The framework of $(Me_2NH_2)[In(ABDC)_2]$ viewed down the *c*-axis showing the interwoven helical struture of the interpentrated chains that define the pores (shaded in blue) along the *a*-axis

Previous studies of the framework using volumetric adsorption measurements reported that the MOF exhibits excellent CO_2 *vs* CH_4 selectivity,[1] implying the channels are of suitable size for a molecular sieving effect. This chapter will focus on the structural effects of removing the guest DMF molecules, which is required before gaseous uptake, showing that this pore size is actually variable. This will be carried out through crystallographic studies using a combination of *in situ* and *ex situ* heating techniques. The gas uptake properties of the framework are directly affected by the results shown in the chapter and will be described in chapter 4.

2.3 Experimental

2.3.1 General

All reagents were purchased from Sigma-Aldrich or Alfa Aesar and were used without further purification, unless otherwise stated. Elemental analyses were recorded on a Perkin Elmer 24000 CHNS/O Series II Elemental Analyser using combustion in pure oxygen.

2.3.2 Synthesis

Synthesis of $(Me_2NH_2)[In(ABDC)_2].xDMF.yH_2O$

N,N-dimethylformamide (DMF) (10 mL) was added to a mixture of $InCl_3$ (0.1106 g 0.5 mmol) and 2-aminoterephthalic acid (0.092 g, 0.5 mmol) and stirred until fully dissolved. The solution was then transferred to a 100 mL Teflon-lined steel autoclave and placed inside a temperature-controlled oven. The temperature was ramped to 130 ^oC at 1 ^oC/min and maintained for 24 h before cooling to room temperature at a rate of 0.1 ^oC/min. The solvent was decanted off and the brown-octahedron-shaped crystals were transferred and stored in fresh DMF (Yield: 46 % assuming 1.75 DMF and 1.25 H_2O per indium centre as suggested by elemental analysis).

Elemental analysis calculated for $(Me_2NH_2)[In(ABDC)_2]\cdot1.75DMF\cdot1.25H_2O$: C, 41.70; H, 4.93; N, 9.94. Found C, 41.69; H, 4.93; N, 9.92

Synthesis of $[InH(BDC)_2].xDMF.yH_2O$ (QMOF2)

N,N-dimethylformamide (DMF) (10 mL) was added to a mixture of $InCl_3$ (0.1106 g, 0.5 mmol) and terephthalic acid (0.085g, 0.5 mmol) and stirred until fully dissolved. The solution was then transferred to a 100 mL Teflon-lined steel autoclave and placed inside a temperature-controlled oven. The temperature was ramped to 130 ^oC at 1 ^oC/min and maintained for 24 h before cooling to room temperature at a rate of 0.1 ^oC/min. The solvent was filtered off leaving a fine white powder (Yield: 20.5 % assuming 2.75 DMF and 3.5 H_2O per indium centre as suggested by elemental analysis).

Elemental analysis calculated for $[InH(BDC)_2]\cdot2.75DMF\cdot3.5H_2O$: C, 41.13; H, 5.02; N, 5.44. Found C, 41.21; H, 5.08; N, 5.36

2.3.3 Analysis

TGA analyses were obtained using a Perkin Elmer Thermogravimetric Analyser under a nitrogen atmosphere. The sample (2.5 mg) was heated from 25°C to 600°C at a rate of 3 °C/min and the exported data was plotted using Microsoft Excel.

Solid-State IR was recorded using a PerkinElmer spectrum 100 spectrometer fitted with a universal diamond ATR accessory.

Solution-phase ^{1}H NMR spectroscopy (400 MHz, DMSO-d6) was carried out using a Bruker DPX-400 spectrometer. The MOF sample (10 mg) was digested using 50 µL of acid (35% DCl in D_2O) in 1 mL of DMSO-d6, and recorded without neutralising the solution. All the constituent parts were observed to be soluble in the DMSO after the digestion.

Laboratory single-crystal X-ray diffraction data were collected on a Bruker SMART APEX-II CCD diffractometer operating a Mo-K_α sealed-tube X-ray source or a Bruker D8 Venture diffractometer equipped with a PHOTON 100 dual-CMOS chip detector and operating a Cu-K_α IµS microfocus X-ray source. The data were processed using the APEX2 software.[10] An Oxford Cryosystems Cryostream device was used to maintain the sample temperature. X-Ray data were corrected for absorption using empirical methods (SADABS) based upon symmetry-equivalent reflections combined with measurements at different azimuthal angles.[11, 12] All crystal structures were solved and refined against F^2 values using the SHELX 2013 suite accessed within the OLEX2 program.[13, 14] Non-disordered, non-hydrogen framework atoms were refined anisotropically, but disordered framework atoms and cations were modelled with isotropic displacement parameters, using a combination of crystallographic restraints and constraints. Hydrogen atoms were placed in calculated positions with idealised geometries and then refined using a riding model with isotropic displacement parameters. Final CIFs were checked using checkCIF/PLATON.[9] The routine SQUEEZE in the program PLATON was used to obtain a residual electron count within the pore, but was not used in the structure refinements.[8] All electron counts were obtained after fully removing any modelled counter ions from the crystallographic model and re-refining the structure. The electron count associated with the solvent was then determeined by manually subtracted the number of electrons from the counterions away from the total contained within the unit cell.

Laboratory powder diffraction data were obtained using a Bruker D8 Advance powder diffractometer equipped with focusing Göbel mirrors, recorded in the range $4^\circ \leq 2\theta \leq 50^\circ$, using Cu-$K_\alpha$ radiation. Data were collected in a Debye-Scherrer geometry with rotating capillary stage and samples loaded in either 0.5 mm or 0.7 mm borosilicate capillaries. Sample temperature for *in situ*

heating studies was controlled by a co-axial stream of dry nitrogen gas from an Oxford Cryosystems Cryostream Plus device, with a flow rate of 5 L/min. Synchrotron powder diffraction data were collected at beamline I11 at Diamond Light Source using a wide-angle (90 °) position sensitive detector (PSD) comprising 18 Mythen-2 modules.[15, 16] A pair of scans related by a 0.25 ° detector offset was collected for each measurement to account for gaps between detector modules. The resulting patterns were summed to give the final pattern for analysis. All ambient pressure data were collected in transmission geometry using either 0.5 or 0.7 mm diameter borosilicate tubes. Indexing, Pawley[17] and Rietveld[18–20] refinements were carried out using TOPAS version 4.1[21] Measures of agreement between the calculated and experimental diffraction data (R_{wp} and R_{wp}') are defined by the equations below.

$$R_{wp} = \sqrt{\frac{\Sigma[w(Y_{\mathrm{obs}} - Y_{\mathrm{calc}})^2]}{\Sigma[wY_{\mathrm{obs}}{}^2]}} \qquad R_{wp}{}' = \sqrt{\frac{\Sigma[w(Y_{\mathrm{obs}} - Y_{\mathrm{calc}})^2]}{\Sigma[w(Y_{\mathrm{obs}} - bkgr)^2]}}$$

2.3.4 Crystal structures of as-synthesised MOF $(Me_2NH_2)[In(ABDC)_2]$

Crystal structures of the as-synthesised MOF $(Me_2NH_2)[In(ABDC)_2]$ (in DMF/H_2O-solvated form) were obtained by transferring the single crystals obtained from the synthesis directly into a perfluoropolyether oil (FOMBLIN Y), mounting a suitable crystal onto a MiTeGen 200µm MicroMount under an optical microscope, and transferring this to the diffractometer where the crystal was immersed in the dry nitrogen stream of the Crysotream device at 100 K. Three crystal structures were obtained from three different synthetic batches, and crystal data are shown in Table 2. Analysis of the electron density in the pore was determined using SQUEEZE[8] and is shown in Table 1.

Table 1 – Electron count from SQUEEZE analysis of as-synthesised MOF $(Me_2NH_2)[In(ABDC)_2]$

	Electrons per unit cell (in void spaces)	Solvent accessible void per unit cell (Å^3)	Electrons per Indium due to solvent [a]
1	1932	7064.3	94
2	2304	6966.6	117
3	1981	7041.8	97

[a] Calculated by dividing the electron count per cell by Z and subtracting the electrons associated with the cations

Table 2 - Data collection, structure solution and refinement parameters for single crystal X-ray structure determinations of as-synthesised MOF $(Me_2NH_2)[In(ABDC)_2]$

	As synthesised MOF-1 **(1)**	As synthesised MOF-2 **(2)**	As synthesised MOF-3 **(3)**
Crystal Habit	Octahedron	Octahedron	Octahedron
Crystal Colour	Brown	Brown	Brown
Crystal Size (mm)	0.27 x 0.17 x 0.10	0.4 x 0.35 x 0.28	0.50 x 0.35 x 0.25
Crystal System	Orthorhombic	Orthorhombic	Orthorhombic
Space Group, Z	*Fddd*, 16	*Fddd*, 16	*Fddd*, 16
a (Å)	15.3069(5)	15.2451(4)	15.155(3)
b (Å)	26.9467(8)	26.7998(8)	26.139(6)
c (Å)	31.284 (1)	31.3225(8)	31.908(7)
α (°)	90	90	90
β (°)	90	90	90
γ (°)	90	90	90
V (Å^3)	12903.7(3)	12797.3(6)	12640(5)
Radiation	Mo-K_α (λ = 0.71073 Å)	Mo-K_α (λ = 0.71073 Å)	Mo-K_α (λ = 0.71073 Å)
Density (g cm^{-3})[b]	1.069	1.078	1.091
Temperature (K)	100	100	100
μ (mm^{-1})[c]	0.765	0.771	0.781
2θ Range (°)	3.32 to 55.06	3.34 to 55.28	3.36 to 55.32
Reflns collected	43105	30244	25258
Independent reflns (R_{int})	3725 (0.0268)	3718 (0.0319)	3679 (0.0961)
Reflns used in refinement, *n*	3725	3718	3679
L.S. parameters, *p*	139	139	128
No. of restraints, *r*	8	8	6
Completeness	0.999	0.995	0.994
*R*1(*F*)[a] $I > 2\sigma(I)$	0.0525	0.0501	0.0961
*wR*2(F^2)[a], all data	0.1962	0.2092	0.3217
S(F^2)[a], all data	1.205	1.231	1.067

[a] $R1(F) = \sum(|F_o| - |F_c|)/\sum|F_o|$; $wR2(F^2) = \sqrt{\sum w\left(F_o^2 - F_c^2\right)^2/\sum wF_o^4}$; $S(F^2) = \sqrt{\sum w\left(F_o^2 - F_c^2\right)^2/(n+r-p)}$.

[b] Densities are calculated using only framework atoms and cations, and do not include guest molecules.

[c] Adsorption coefficients are calculated based on the crystallographic model

2.3.5 Bulk phase analysis of as-synthesised $(Me_2NH_2)[In(ABDC)_2]$

The phase purity of the framework was confirmed through X-ray powder diffraction. A room temperature pattern (**P1**) was collected at the I11 beamline[15, 16] as detailed in Section 2.3.3, λ = 0.82562(2) Å. The unit cell parameters from the single crystal structure of the as-synthesised MOF (**1**) were used as starting point for a Pawley refinement, employing 1,040 parameters (12 background, 1 zero error, 5 profile, 3 cell and 1,019 reflections), resulting in final indices of fit R_{wp} = 3.524, $R_{wp'}$ = 7.872. The framework atoms of **1** were then used as a starting point for a Rietveld refinement employing 24 parameters (12 background, 1 zero error, 5 profile, 3 cell, 1 scale, 2 occupancies), resulting in final indices of fit R_{wp} = 8.799, $R_{wp'}$ = 20.047. The fits are shown in Figure 4 and Figure 5. The positions and orientations of the cation and solvent molecules (modelled as rigid bodies) were optimised by simulated annealing. The final unit cell parameters were orthorhombic *a* = 15.4972 (3) Å, *b* = 27.0405 (7) Å, *c* = 31.1936 (8) Å, *V* = 13071.7 (6) Å^3.

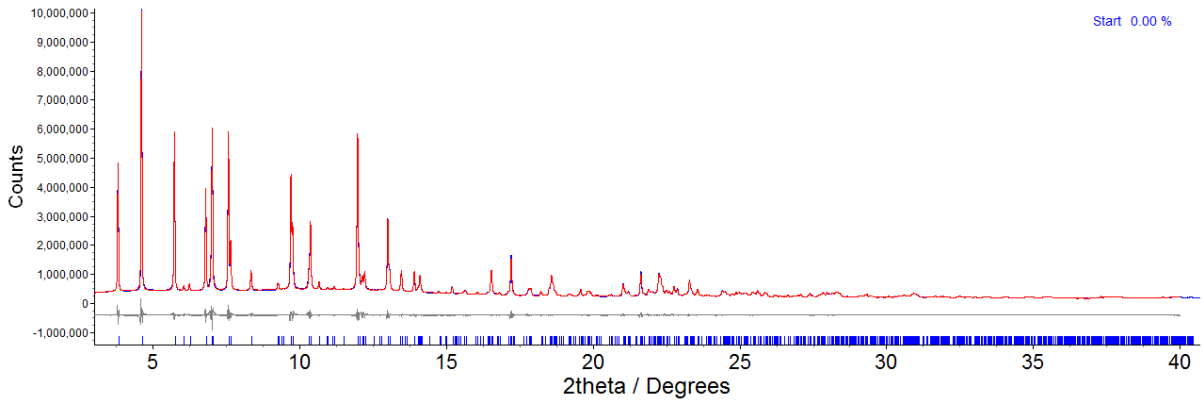

Figure 4 – Observed (blue) and calculated (red) and difference plot [I_{obs}-I_{calc}] (grey) of the Pawley[17] refinement of as-synthesised $(Me_2NH_2)[In(ABDC)_2]$ **P1** (2θ range 3.0 – 40.0 °, d_{min} = 1.2Å).

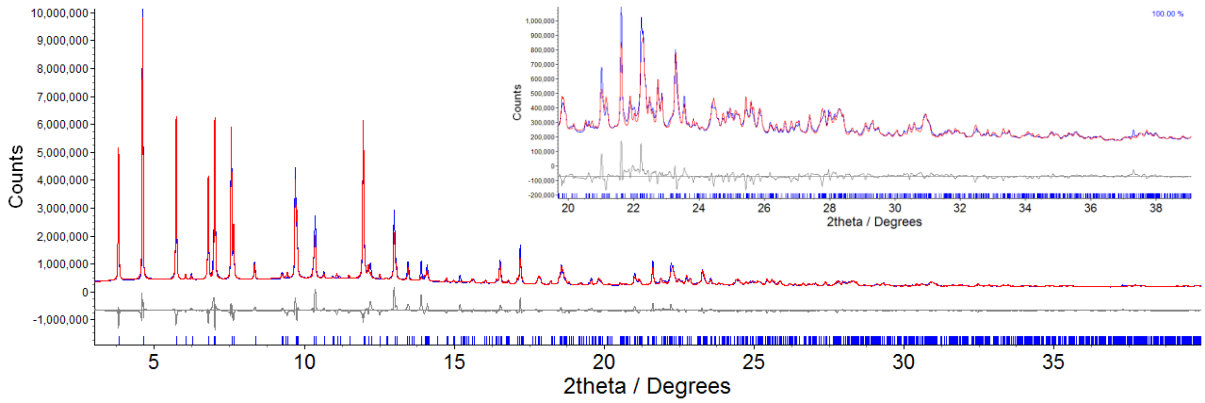

Figure 5 – Observed (blue) and calculated (red) and difference plot [I_{obs}-I_{calc}] (grey) of the Rietveld[20] refinement as-synthesised $(Me_2NH_2)[In(ABDC)_2](0.75DMF)(0.25H_2O)$ **P1** (2θ range 3.0 – 40.0 °, d_{min} = 1.2Å).

2.3.6 Bulk phase analysis of as-synthesised [InH(BDC)$_2$] (QMOF2)

The identity of the framework formed from reactions of terephthalic acid with $InCl_3$ in the analogous synthesis to that used to prepare $(Me_2NH_2)[In(ABDC)_2]$ was confirmed through X-ray powder diffraction. A room temperature pattern was collected at the I11 beamline as detailed in Section 2.3.3, λ = 0.82562(2) Å. This pattern was compared to patterns calculated from single crystal structures deposited in Cambridge Structural Database. The powder pattern was found to be a good match to that of the MOF [InH(BDC)$_2$], known as QMOF2.[22] The differences are likely to arise from an absence of modelling of the pore contents in QMOF2 and the difference in temperature between the two diffraction measurements. The predicted and experimental powder diffraction patterns are displayed in Figure 6.

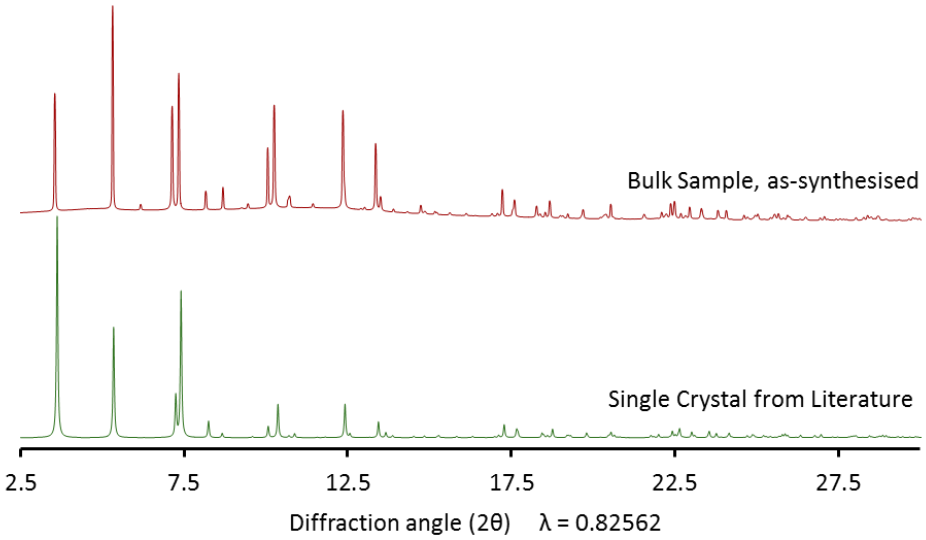

Figure 6 - Experimental X-ray powder diffraction pattern of the product of solvothermal synthesis using $InCl_3$ and terepthalic acid compared to the predicted pattern of the MOF QMOF2.[22]

2.3.7 *Ex situ* solvent removal studies on single crystals of as-synthesised $(Me_2NH_2)[In(ABDC)_2]$

Crystals of as-synthesised $(Me_2NH_2)[In(ABDC)_2]$ were transferred from the DMF solvent to a microscope slide and left until the DMF had evaporated. The crystals were then either heated or left to dry in air for a fixed period of time as summarised in Table 3. After treatment the crystals were covered in a perfluoropolyether oil and mounted on a goniometer head. X-Ray diffraction data were recorded at reduced temperatures (100-120 K) under a cold nitrogen stream. The crystals retained most of their crystallinity, enabling detailed structural information to be obtained. Full crystallographic information for these structures is listed in Table 4 and Table 5 and analysis of the electron dentistry in the solvent accessible void by the routine SQUEEZE[8] in the program PLATON is displayed in Table 6.

Table 3 - Treatment methods used in ex situ desolvation studies of single crystal $(Me_2NH_2)[In(ABDC)_2]$

Crystal No.	Treatment Method
4	Dried in Air 2 hours
5	Dried in Air 14hrs
6	Heated to 100 ^oC for 10 mins
7	Heated to 150 ^oC for 5 mins
8	Heated to 150 ^oC for 5 mins
9	Heated to 150 ^oC for 15 mins
10	Heated to 150 ^oC for 15 mins, left in air for 2 days

Table 4 - Data collection, structure solution and refinement parameters for *ex situ* solvent removal studies on as-synthesised $(Me_2NH_2)[In(ABDC)_2]$, part 1

	Dried in air for 2 hours **(4)**	Dried in air overnight **(5)**	Heated to 100 °C for 10 mins**(6)**	Heated at 150 °C for 5 min **(7)**
Crystal Habit	Octahedron	Octahedron	Octahedron	Octahedron
Crystal Colour	Brown	Brown	Brown	Brown
Crystal Size (mm)	0.40 x 0.30 x 0.16	0.54 x 0.38 x 0.30	0.18 × 0.14 × 0.08	0.50 x 0.30 x 0.15
Crystal System	Orthorhombic	Orthorhombic	Orthorhombic	Orthorhombic
Space Group, Z	*Fddd*, 16	*Fddd*, 16	*Fddd*, 16	*Fddd*, 16
a (Å)	15.1230(7)	15.1046(4)	15.151(4)	14.9603(4)
b (Å)	23.056(1)	24.5318(7)	23.282(7)	21.8384(6)
c (Å)	34.0427(14)	33.1539(9)	33.961(14)	34.7768(9)
α (°)	90	90	90	90
β (°)	90	90	90	90
γ (°)	90	90	90	90
V (Å^3)	11870.1(9)	12284.9(6)	11979(7)	11361.9(5)
Radiation	Mo-K_α (λ = 0.71073 Å)	Mo-K_α (λ = 0.71073 Å)	Cu-K_α (λ = 1.54178 Å)	Mo-K_α (λ = 0.71073 Å)
Density (g cm^{-3})[b]	1.162	1.123	1.152	1.214
Temperature (K)	118	108	100	100
μ (mm^{-1})[c]	0.831	0.803	6.622	0.868
2θ Range (°)	3.44 to 55.04	3.4 to 55.12	7.44 to 133.4	3.5 to 54.98
Reflns collected	40370	27316	19615	26643
Independent reflns (R_{int})	3422 (0.0312)	3551 (0.0435)	2659 (0.0537)	3259 (0.0622)
Reflns used in refinement, *n*	3422	3551	2659	3259
L.S. parameters, *p*	117	143	147	125
No. of restraints, *r*	6	4	6	20
Completeness	0.999	0.996	0.995	0.994
$R1(F)$[a] $I > 2\sigma(I)$	0.0674	0.0776	0.0719	0.0944
$wR2(F^2)$[a], all data	0.2549	0.3042	0.2271	0.3158
$S(F^2)$[a], all data	1.157	1.224	1.108	1.242

[a] $R1(F) = \sum(|F_o| - |F_c|)/\sum|F_o|$; $wR2(F^2) = \sqrt{\sum w\left(F_o^2 - F_c^2\right)^2/\sum wF_o^4}$; $S(F^2) = \sqrt{\sum w\left(F_o^2 - F_c^2\right)^2/(n+r-p)}$.

[b] Densities are calculated using only framework atoms and cations, and do not include guest molecules.

[c] Adsorption coefficients are calculated based on the crystallographic model

Table 5 - Data collection, structure solution and refinement parameters for *ex situ* solvent removal studies on as-synthesised $(Me_2NH_2)[In(ABDC)_2]$, part 2

	Heated at 150 °C for 5 min **(8)**	Heated at 150 °C for 15 min **(9)**	Heated at 150 °C for 15 min then left in air for 2 days **(10)**
Crystal Habit	Octahedron	Octahedron	Octahedron
Crystal Colour	Brown	Brown	Brown
Crystal Size (mm)	0.60 x 0.30 x 0.30	0.66 x 0.44 x 0.37	0.51 x 0.51 x 0.24
Crystal System	Orthorhombic	Orthorhombic	Orthorhombic
Space Group, Z	*Fddd*, 16	*Fddd*, 16	*Fddd*, 16
a (Å)	14.900(3)	14.8498(7)	15.0954(14)
b (Å)	21.816(5)	20.9133(13)	25.789(2)
c (Å)	34.796(7)	35.2975(16)	32.274(3)
α (°)	90	90	90
β (°)	90	90	90
γ (°)	90	90	90
V (Å^3)	11311(4)	10961.9(10)	12564(2)
Radiation	Mo-K_α (λ = 0.71073 Å)	Mo-K_α (λ = 0.71073 Å)	Mo-K_α (λ = 0.71073 Å)
Density (g cm^{-3})[b]	1.220	1.258	1.098
Temperature (K)	100	105	108
μ (mm^{-1})[c]	0.872	0.900	0.785
2θ Range (°)	3.52 to 55.1	3.56 to 55.12	3.38 to 54.9
Reflns collected	20453	20534	21669
Independent reflns (R_{int})	3255 (0.1159)	3162 (0.1032)	3594 (0.0861)
Reflns used in refinement, *n*	3255	3162	3594
L.S. parameters, *p*	121	140	121
No. of restraints, *r*	10	5	9
Completeness	0.994	0.998	0.998
*R*1(F)[a] $I > 2\sigma(I)$	0.1221	0.101	0.0756
*wR*2(F^2)[a], all data	0.4199	0.3644	0.2908
S(*F*^{2})[a], all data	1.245	1.066	1.074

[a] $R1(F) = \sum(|F_o| - |F_c|)/\sum|F_o|$; $wR2(F^2) = \sqrt{\sum w\left(F_o^2 - F_c^2\right)^2/\sum wF_o^4}$; $S(F^2) = \sqrt{\sum w\left(F_o^2 - F_c^2\right)^2/(n+r-p)}$.

[b] Densities are calculated using only framework atoms and cations, and do not include guest molecules.

[c] Adsorption coefficients are calculated based on the crystallographic model

Table 6 – Electron count from SQUEEZE analysis of *ex situ* heated as-synthesised MOF $(Me_2NH_2)[In(ABDC)_2]$

	Electrons per unit cell (in void spaces)	Solvent accessible void per unit cell ($Å^3$)	Electrons per Indium due to solvent [a]
4	1909	5895.1	92
5	1916	5987.5	93
6	1634	5720.4	75
7	1467	4681.6	65
8	1186	5496.7	47
9	1136	4845.3	44
10	1727	6464.1	81

[a] Calculated by dividing the electron count per unit cell by Z and subtracting the electrons associated with the cations

2.3.8 Crystallographic studies of as-synthesised $(Me_2NH_2)[In(ABDC)_2]$ using *in situ* heating

In situ diffraction

Crystals used for *in situ* heating were selected while immersed in the mother liquor and one face of the crystal was glued to a glass fibre while the crystal was still covered in a thin layer of residual solvent. Care was taken to avoid coating the entire crystal in adhesive. The crystal was rapidly transferred to the diffractometer and situated in the nitrogen stream of the Cryostream device at room temperature. The glue was left to dry for 15 mins before any data were collected. Heating was carried out *in situ* using the Cryostream device. Three different heating experiments were carried out on three separate crystals (**H1**, **H2** and **H3**). A ramp rate of 2 °C/min (**H1**) or 4 °C/min (**H2** and **H3**) was used to raise the temperature, which was held at the final value for a fixed period (see Table 7) before cooling at the same ramp rate. Intensity data collections were recorded under the nitrogen stream at 298 K, using the Cryostream to maintain the temperature. The unit cell parameters were obtained by analysing reflections of I/σ > 10 from 4 sets of 10° omega scans with 0.5° slicing. Full data collections were recorded at the end of the studies **H1** and **H2** due to the sample maintaining a high level of crystallinity (**H1.6** and **H2.2**). Table 7 details the 3 separate heating studies carried out and the resulting cell parameters. The details of the full data collections at the end of studies **H1** and **H2** are shown in Table 9 and analysis of the electron density in the solvent accessible void using the SQUEEZE[8] routine is displayed in Table 8.

Table 7 - Parameters used and unit cell determined for crystallographic studies of desolvation by in situ heating

Heating Study No. (ramp rate)	Temp heated	Hold time	Data set Code	*a* (Å)	*b* (Å)	*c* (Å)	*V* (Å^3)
1 (2 °C/min)	25 °C	Start	**H1.1**	15.460(7)	27.214(6)	31.029(6)	13055(8)
	40 °C	5 mins	**H1.2**	15.553(6)	26.88(1)	31.244(7)	13062(9)
	60 °C		**H1.3**	15.21(1)	23.77(1)	33.61(1)	12147(12)
	80 °C		**H1.4**	15.22(1)	23.45(1)	33.847(9)	12079(10)
	100 °C		**H1.5**	15.182(8)	22.991(7)	34.116(7)	11909(8)
	120 °C		**H1.6**	15.142(8)	22.235(13)	34.53(2)	11624(11)
2 (4 °C/min)	25 °C	Start	**H2.1**	15.449(4)	27.125(6)	31.125(12)	13043(7)
	150 °C	5 mins	**H2.2**	15.158(5)	22.565(8)	34.411(12)	11770(7)
3 (4 °C/min)	25 °C	Start	**H3.1**	15.488(3)	27.206(7)	31.055(7)	13086(5)
	150 °C	15 mins	**H3.2**	15.043(6)	21.666(7)	34.867(7)	11364(7)

All data recorded at 298K

Table 8 – Electron count from SQUEEZE analysis of as-synthesised MOF $(Me_2NH_2)[In(ABDC)_2]$

	Electrons per unit cell (in void spaces)	Solvent accessible void per unit cell (Å^3)	Electrons per Indium due to solvent [a]
H1.6	949	5659.7	32
H2.2	623	5814.9	12

[a] Calculated by dividing the electron count per unit cell by Z and subtracting the electrons associated with the cations

Images of crystals

Images of the crystals during *in situ* heating experiment 3 (**H3.1** and **H3.2**) were obtained using the camera on the diffractometer. The images were obtained at the same diffractometer angles and are shown in Figure 7. No adjustment to the crystal position was made during the study.

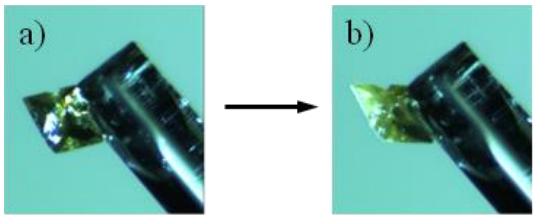

Figure 7 – Images obtained for experiments a) **H3.1** and b) **H3.2** during *in situ* heating experiment 3

Table 9 - Data collection, structure solution and refinement parameters of single crystal diffraction data **9-12**

	In situ heating of as-synthesised MOF - 1 **(H1.6)**	*In situ* heating of as-synthesised MOF - 2 **(H2.2)**
Crystal Habit	Octahedron	Octahedron
Crystal Colour	Brown	Brown
Crystal Size (mm)	0.23 × 0.20 × 0.14	0.34 × 0.24 × 0.18
Crystal System	Orthorhombic	Orthorhombic
Space Group, Z	*Fddd*, 16	*Fddd*, 16
a (Å)	15.142(8)	15.158(5)
b (Å)	22.235(13)	22.565(8)
c (Å)	34.53(2)	34.411(12)
α (°)	90	90
β (°)	90	90
γ (°)	90	90
V (Å^3)	11624(11)	11770(7)
Radiation	Cu-K_α (λ = 1.54178 Å)	Cu-K_α (λ = 1.54178 Å)
Density (g cm^{-3})[b]	1.187	1.172
Temperature (K)	298	298
μ (mm^{-1})[c]	6.825	6.757
2θ Range (°)	7.52 to 134.2	7.48 to 133.28
Reflns collected	14608	14432
Independent reflns (R_{int})	2584 (0.0608)	2597 (0.0605)
Reflns used in refinement, *n*	2584	2597
L.S. parameters, *p*	143	145
No. of restraints, *r*	6	5
Completeness	0.990	0.995
$R1(F)$[a] $I > 2\sigma(I)$	0.0808	0.0747
$wR2(F^2)$[a], all data	0.2464	0.2365
$S(F^2)$[a], all data	1.127	1.125

[a] $R1(F) = \sum(|F_o| - |F_c|)/\sum|F_o|$; $wR2(F^2) = \sqrt{\sum w\left(F_o^2 - F_c^2\right)^2/\sum wF_o^4}$; $S(F^2) = \sqrt{\sum w\left(F_o^2 - F_c^2\right)^2/(n+r-p)}$.

[b] Densities are calculated using only framework atoms and cations, and do not include guest molecules.

[c] Adsorption coefficients are calculated based on the crystallographic model

2.3.9 Complementary Techniques

Solution-phase NMR spectroscopy

Solution-phase ^{1}H NMR spectra of the as-synthesised framework, and the framework after heating at 150 ^{o}C for 15 mins, were obtained following digestion using the method described in Section 2.3.3. The spectrum of the as-synthesised MOF is shown together with an enlarged section showing only the aromatic protons in Figure 8 and Figure 9, and spectrum of the heated MOF along with its enlarged section is shown in Figure 10 and Figure 11. The integrations of the aromatic protons on the ligand were compared to the carbonyl and methyl protons of the DMF to quantify the amount of contained solvent. This suggested 2 DMF molecules per indium in the as-synthesised framework and 0.55 DMF molecules per indium after heat treatment. NH_2 protons were not observed in the spectra due to exchange with the D_2O present.

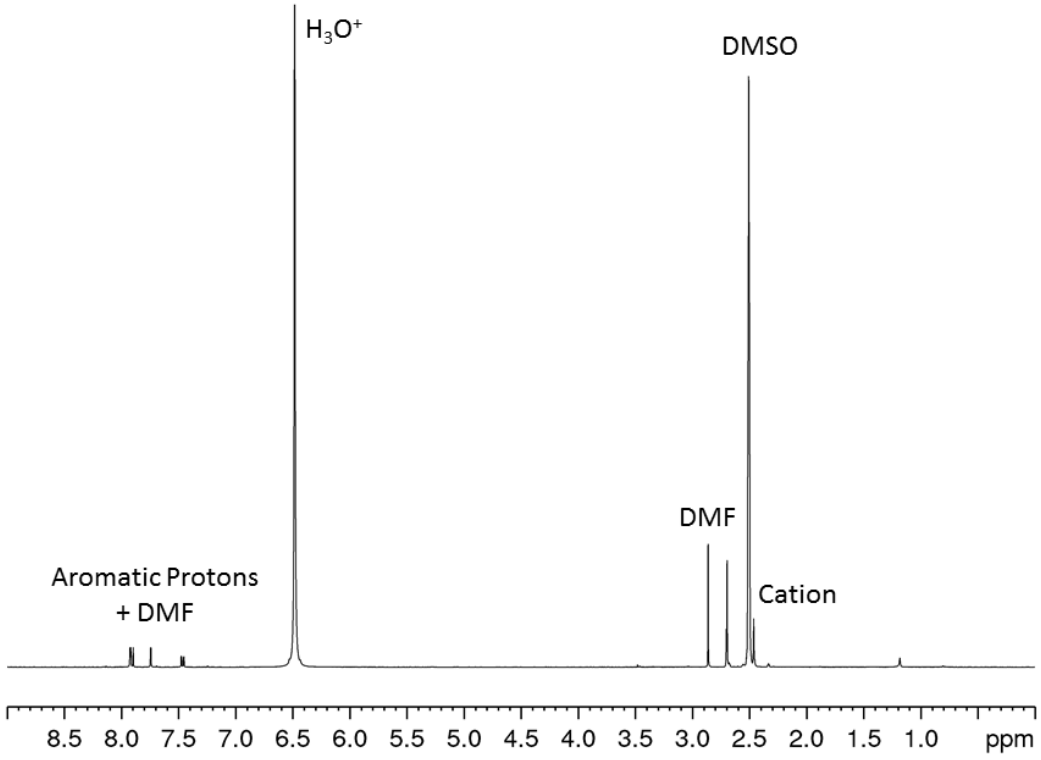

Figure 8 – Solution phase ^{1}H NMR spectrum of the as-synthesised framework $(Me_2NH_2)[In(ABDC)_2]$ after digestion

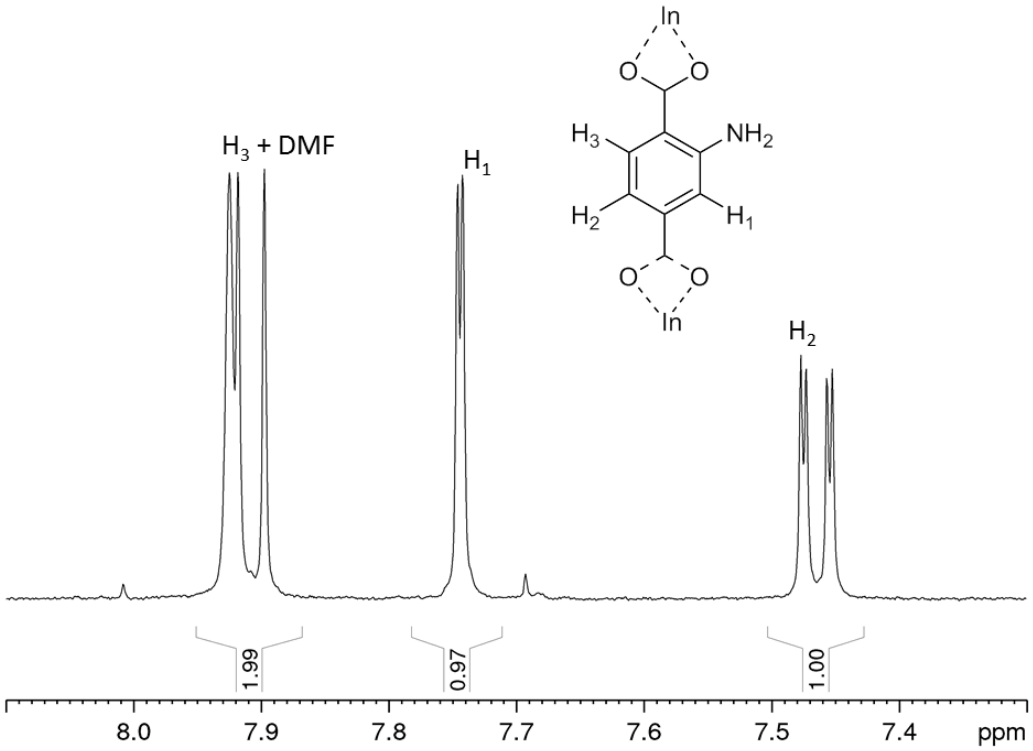

Figure 9 - Expanded Range of the solution phase ^{1}H NMR spectrum of the as-synthesised framework $(Me_2NH_2)[In(ABDC)_2]$ after digestion

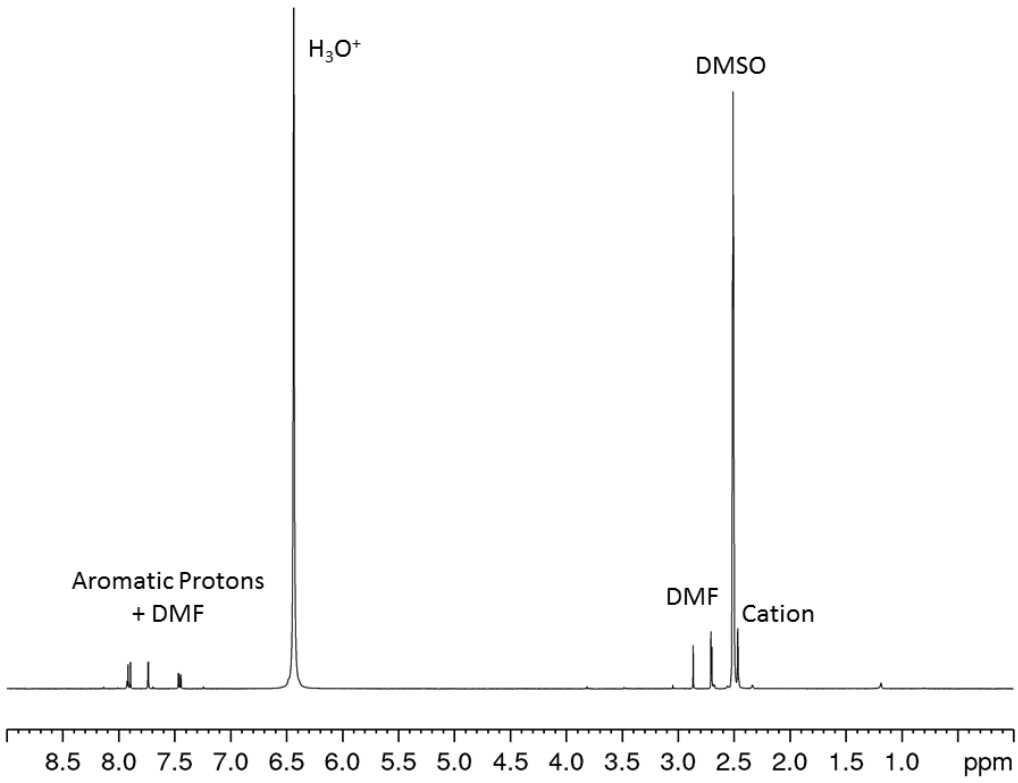

Figure 10 – Solution phase ^{1}H NMR spectrum of as-synthesised framework $(Me_2NH_2)[In(ABDC)_2]$ after heating at 150 ^{o}C for 15 mins and digestion

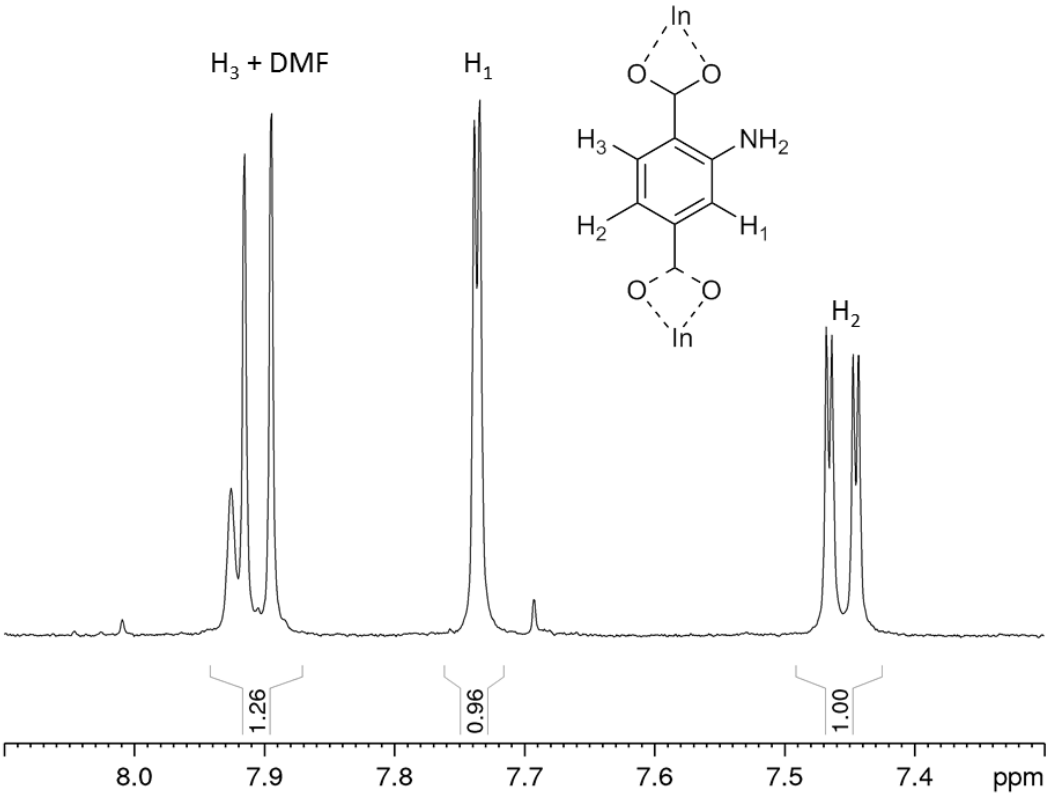

Figure 11 – Expanded range of solution phase ^{1}H NMR spectrum of as-synthesised framework $(Me_2NH_2)[In(ABDC)_2]$ after heating at 150 ^{o}C for 15 mins and digestion

Solid state IR spectroscopy

Solid state IR spectra were collected for both the as-synthesised framework and the framework after treatment at 150 °C for 15 mins. The spectra show a significant reduction in the DMF carbonyl band at 1657cm^{-1} after heating of the framework.

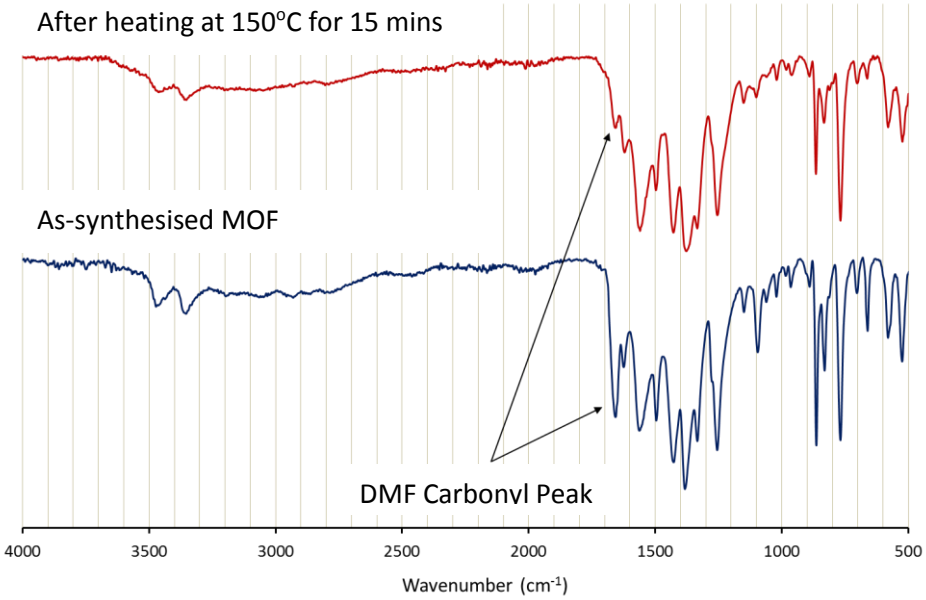

Figure 12 - Solid state IR spectra recorded for as-synthesised In MOF (blue) and after heating at 150 °C for 15 mins (red)

Thermogravimetric analysis

The thermal decomposition of the as-synthesised frameworks under a nitrogen atmosphere was followed using TGA analysis. An example trace is shown in Figure 13 and contains three distinct steps, the first one between 100 °C and 175 °C, the second at about 250 °C, and the final step at 400 °C

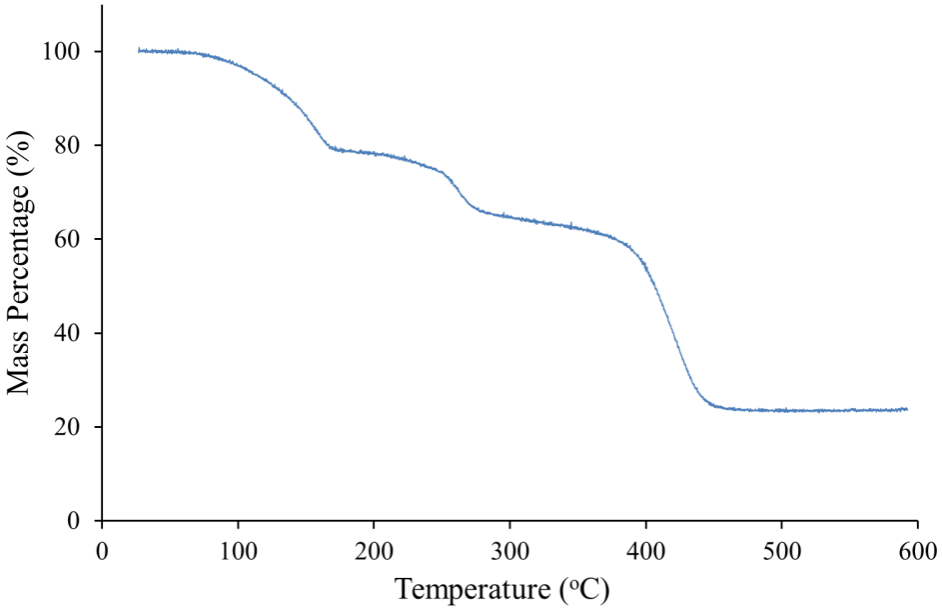

Figure 13 - Thermogravimetric analysis of as-synthesised $(Me_2NH_2)[In(ABDC)_2]$ between 25 °C and 600 °C ramping the temperature at 4 °C/min

2.3.10 Solvent removal studies on powder samples

Solvent removal from the powder (bulk) samples was analysed by Pawley fitting of X-ray powder diffraction patterns obtained after heating using two different procedures (**P2** and **P3**). The results of the fits are shown in Table 10, compared to the refined as-synthesised MOF (**P1**) described in Section 2.3.5. Details of the procedures and fitting are detailed below.

Table 10 - Unit cell parameters of powder samples **P1-3** as-synthesised and heated as-synthesised $(Me_2NH_2)[In(ABDC)_2]$

No.	Treatment	*a* (Å)	*b* (Å)	*c* (Å)	*V* (Å^3)
P1	As-synthesised	15.4972(3)	27.0405(7)	31.1936(8)	13071.7(6)
P2	Heated in Capillary	15.288(3)	23.8417(7)	33.597(1)	12198.4(6)
P3	Heated in inert atmosphere	15.004(3)	21.764(6)	34.838(9)	11377(4)

P2: A sample of as-synthesised $(Me_2NH_2)[In(ABDC)_2]$ was packed into a 0.7mm borosilicate capillary and placed inside a temperature controlled oven. The temperature was raised to 150 °C and held at this temperature for 30 mins. The capillary was subsequently removed from the oven and immediately flame sealed. X-Ray data were collected at room temperature at the I11 beamline[15, 16] at Diamond Light Source as described in Section 2.3.3, λ = 0.82562(2) Å. The unit cell of the MOF was initially determined by analysis of the positions of the first few Bragg reflections and their known Miller indices. These unit cell parameters were used as a starting point for the Pawley refinement employing 978 parameters (10 background, 1 zero error, 5 profile, 3 cell, 959 reflections), resulting in final indices of fit R_{wp} = 5.949 and $R_{wp'}$ = 12.114. The final unit cell parameters were orthorhombic *a* = 15.2288 (3) Å, *b* = 23.8417 (7) Å, *c* = 33.597 (1) Å, *V* = 12198.4 (6) Å^3. The fit is shown in Figure 14

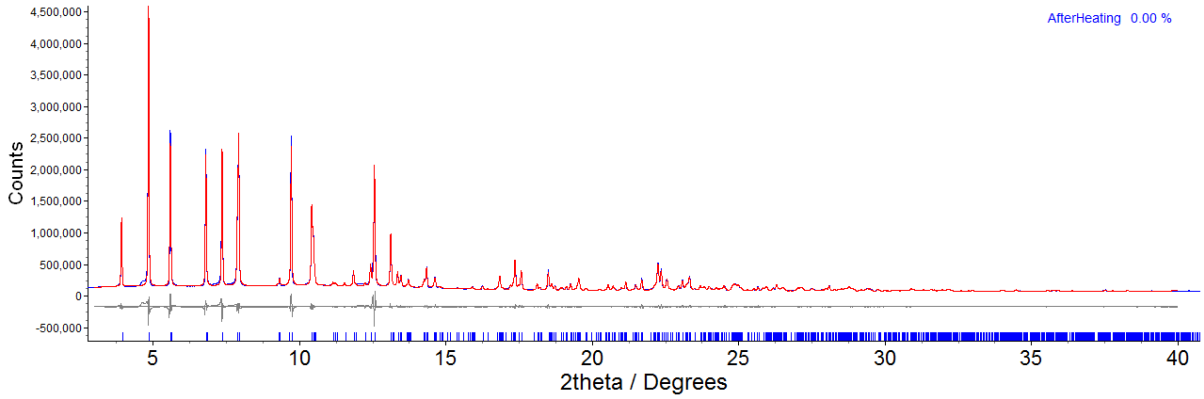

Figure 14 - Observed (blue) and calculated (red) profiles and difference plot [I_{obs}-I_{calc}] (grey) for the Pawley[17] refinement of capillary heated as-synthesised $(Me_2NH_2)[In(ABDC)_2]$ (2θ range 3.0 – 40.0 °, d_{min} = 1.2Å).

P3: As-synthesised $(Me_2NH_2)[In(ABDC)_2]$ was heated to 150 °C, while located in a Schlenk tube under constant nitrogen flow, prior to packing the sample into a 0.7mm borosilicate capillary in an argon filled glovebox. This avoided contact of the sample with atmospheric water vapour, the capillary was flame sealed immediately upon removal from the glovebox. X-ray data were collected on a Bruker D8 diffractometer using Cu-K_α radiation at room temperature. The unit cell of the MOF was approximately determined by analysis of the positions of the first few Bragg reflections and their known Miller indices. These unit cell parameters were used as a starting point for the Pawley refinement employing 169 parameters (9 background, 1 zero error, 6 profile, 3 cell, 96 reflections), resulting in final indices of fit R_{wp} = 6.817 and $R_{wp'}$ = 14.491. The final unit cell parameters were orthorhombic a = 15.004 (3) Å, b = 21.764 (6) Å, c = 34.838 (9) Å, V = 11377 (4) Å^3. The fit is shown in Figure 15.

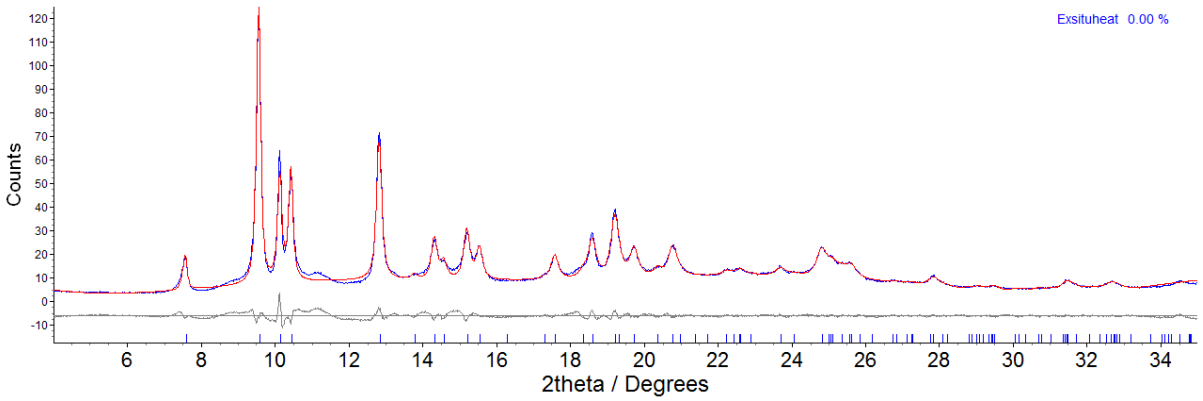

Figure 15 – Observed (blue) and calculated (red) profiles and difference plot [I_{obs}-I_{calc}] (grey) for the Pawley[17] refinement of inert atmosphere heated $(Me_2NH_2)[In(ABDC)_2]$ as-synthesised $(Me_2NH_2)[In(ABDC)_2]$ (2θ range 3.0 – 40.0 °, d_{min} = 2.56Å).

2.3.11 Atmospheric water uptake studies on partially desolvated powder samples

The effect of water uptake by the MOF was monitored by exposing two different partially desolvated MOF samples to atmospheric water vapour while packed inside capillary tubes. One end of the capillary was open to allow a small surface of the material to be exposed to water vapour. The individual experiments are detailed below

Water uptake experiment 1:

A powdered sample of as-synthesised $(Me_2NH_2)[In(ABDC)_2]$ was packed into a 0.5 mm borosilicate capillary with one end left open and mounted on the Bruker D8 Advance diffractometer (Cu-K_α radiation). The nitrogen stream of the Cryostream device was positioned co-axial to the capillary and the temperature ramped to 423 K (150 °C) at 4 °C/ min. The sample was maintained at 150 °C for 20 mins before cooling at a ramp rate of 4 °C/min. A data collection was recorded under the nitrogen stream at 298 K, using the Cryostream to maintain the temperature (**W1.1**). The nitrogen stream was removed, and data continually collected. 5-minute patterns were collected for the first hour, 10-minutes pattern were collected for the second hour and 30-minute patterns were collected for the next 10 hours. The unit cell parameters of patterns at 30-minute intervals (**W1.2** to **W1.24**) were determined using Pawley refinements. The unit cell parameters and final indices of fit are listed in Table 11. **W1.1 – W1.17** were fitted using two-phase Pawley refinements, the minor phase was refined in **W1.1** but fixed for **W1.2 – W1.17**. Extended fitting details are given for representative powder patterns **W1.1**, **W1.12** and **W1.24** only. A stacked plot of the powder diffraction patterns **W1.1** to **W1.24** is shown in Figure 16.

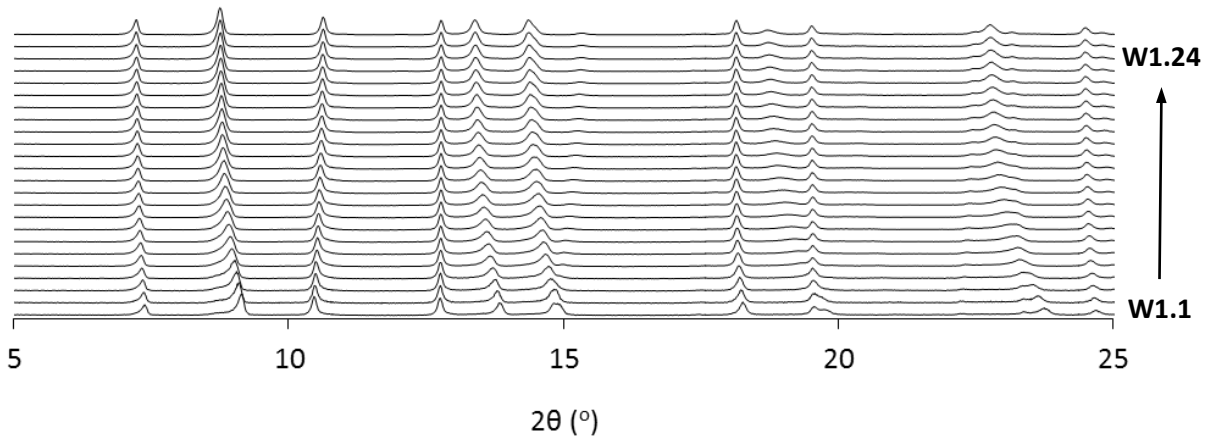

Figure 16 - Powder patterns of partially desolvated as-synthesised $(Me_2NH_2)[In(ABDC)_2]$ recorded at 30 min intervals while exposed to atmospheric water vapour (**W1.1 – W1.24**)

Table 11 - Refined unit cell parameters for water uptake experiment 1 (**W1.1** to **W1.24**)

Code	Scan time	*a* (Å)	*b* (Å)	*c* (Å)	*V* (Å^3)	R_{wp}	$R_{wp'}$
W1.1	10min	15.217(2)	23.827(4)	33.60(1)	12180(8)	7.703	12.703
W1.2	5 min	15.217(1)	23.813(5)	33.61(1)	12177(5)	10.632	16.867
W.13	10 min	15.242(1)	23.989(3)	33.466(7)	12237(3)	8.382	13.168
W.14		15.243(1)	24.210(3)	33.312(5)	12293(2)	9.201	15.238
W1.5	30min	15.2521(9)	24.514(3)	33.134(4)	12388(2)	7.350	12.015
W1.6		15.2562(8)	24.673(3)	33.010(4)	12425(2)	7.201	12.012
W1.7		15.2625(8)	24.806(3)	32.914(4)	12461(2)	7.339	13.407
W1.8		15.2712(9)	24.936(3)	32.819(4)	12497(2)	7.582	13.377
W1.9		15.2785(9)	25.079(3)	32.713(4)	12534(2)	7.736	13.933
W1.10		15.2826(9)	25.179(3)	32.642(4)	12560(2)	7.761	14.085
W1.11		15.2912(9)	25.293(3)	32.558(4)	12592(2)	7.885	14.076
W1.12		15.2974(8)	25.388(3)	32.485(1)	12616(2)	7.621	13.513
W1.13		15.3041(8)	25.473(3)	32.424(3)	12640(2)	7.424	13.700
W1.14		15.3106(8)	25.555(3)	32.365(3)	12663(2)	7.258	13.317
W1.15		15.3168(8)	25.622(3)	32.317(3)	12682(2)	7.090	13.250
W1.16		15.3220(7)	25.684(2)	32.276(3)	12701(2)	6.857	12.935
W1.17		15.3264(7)	25.729(2)	32.241(3)	12713(2)	6.623	12.552
W1.18		15.3349(8)	25.780(2)	32.201(3)	12730(1)	8.925	17.206
W1.19		15.3370(8)	25.817(2)	32.171(3)	12738(2)	8.621	16.595
W1.20		15.3404(8)	25.848(2)	32.148(3)	12747(2)	8.551	16.267
W1.21		15.3431(7)	25.877(2)	32.125(3)	12754(2)	8.296	15.660
W1.22		15.3453(7)	25.903(2)	32.105(3)	12761(2)	8.175	15.438
W1.23		15.3475(7)	25.930(2)	32.087(3)	12769(2)	8.012	15.051
W1.24		15.3497(7)	25.954(2)	32.068(3)	12775(2)	7.833	14.992

All data recorded at 298K

Representative fitting for water uptake experiment 1

W1.1: The unit cell was initially determined by analysis of the positions of the first few Bragg reflections and their known Miller indices. These unit cell parameters were used as a starting point for the two-phase Pawley refinement, employing 582 parameters (9 background, 1 zero error, 5 profile, 6 cell and 557 reflections), resulting in final indices of fit R_{wp} = 7.703, $R_{wp'}$ = 12.703. The final unit cell parameters for the major phase were orthorhombic a = 15.217 (2) Å, b = 23.827 (4) Å, c = 33.60 (1) Å, V = 12180 (8) Å. The minor phase unit cell parameters were orthorhombic a = 15.50 (3) Å, b = 25.89 (3) Å, c = 31.75 (6) Å, V = 12739 (36) Å^3.

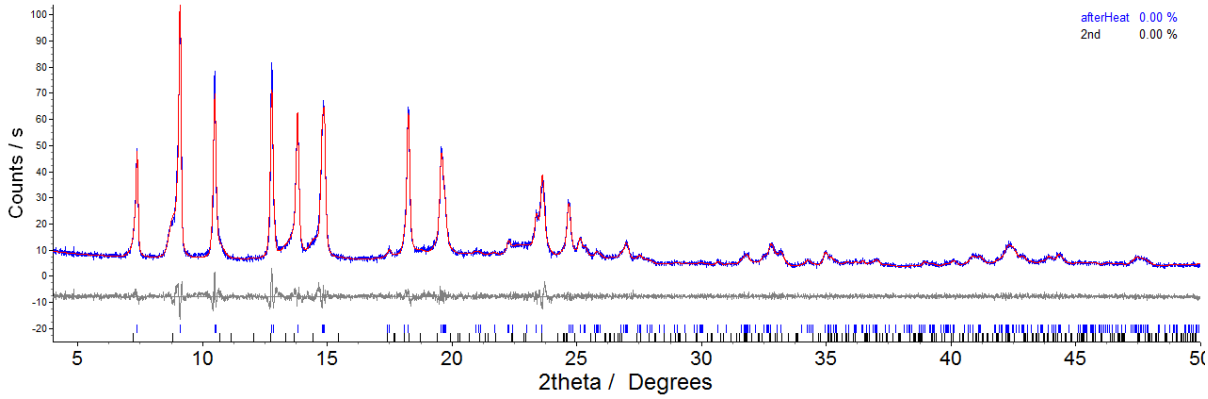

Figure 17 - Observed (blue) and calculated (red) profiles and difference plot [I_{obs}-I_{calc}] (grey) for the Pawley[17] refinement of **W1.1** (2θ range 4.0 – 50.0 °, d_{min} = 1.82Å).

W1.12: The initial starting point for refinement used the unit cell parameters of **W1.11**. The two-phase Pawley refinement employed 587 parameters (6 background, 1 zero error, 5 profile, 3 cell and 572 reflections), resulting in final indices of fit R_{wp} = 7.621, $R_{wp'}$ = 13.513. The final unit cell parameters were orthorhombic a = 15.2974 (8) Å, b = 25.388 (3) Å, c = 32.485 (1) Å, V = 12616 (2) Å. The minor phase was fixed with parameters determined from **W1.1**.

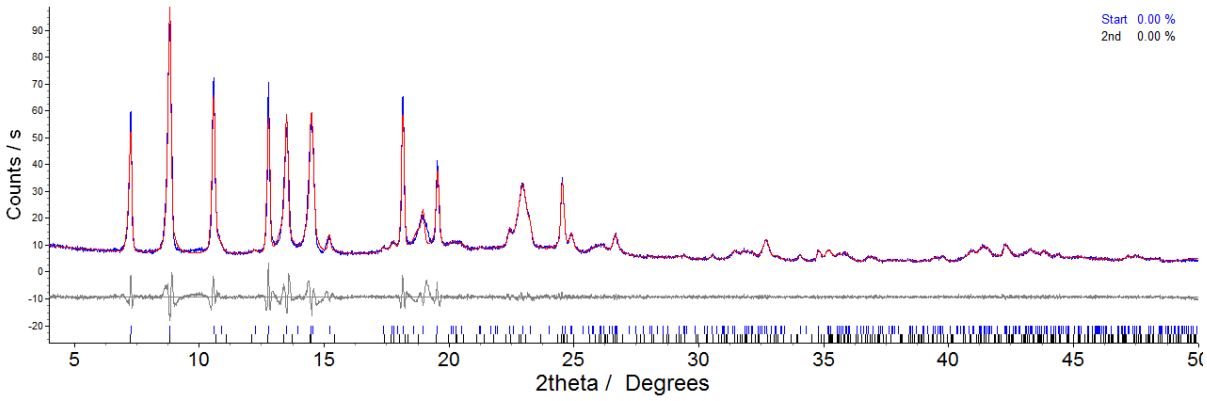

Figure 18 - Observed (blue) and calculated (red) profiles and difference plot [I_{obs}-I_{calc}] (grey) for the Pawley[17] refinement of **W1.12** (2θ range 4.0 – 50.0 °, d_{min} = 1.82Å).

W1.24: The initial starting point for refinement used the unit cell parameters of **W1.23**. The single-phase Pawley refinement employed 306 parameters (6 background, 1 zero error, 5 profile, 3 cell and 291 reflections), resulting in final indices of fit R_{wp} = 7.833, $R_{wp'}$ = 14.992. The final unit cell parameters were orthorhombic a = 15.3497 (7) Å, b = 25.954 (2) Å, c = 32.068 (3) Å, V = 12775 (2) Å^3.

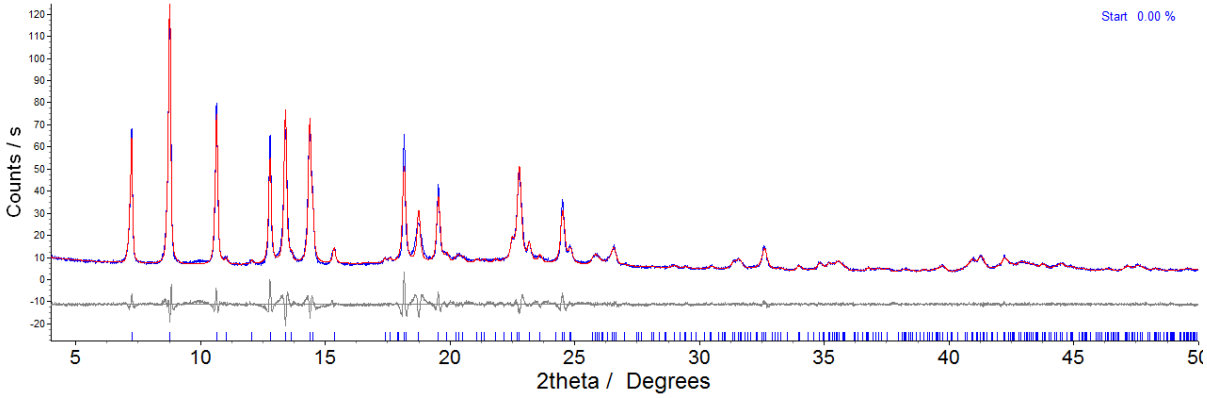

Figure 19 - Observed (blue) and calculated (red) profiles and difference plot [I_{obs}-I_{calc}] (grey) for the Pawley[17] refinement of **W1.24** (2θ range 4.0 – 50.0 °, d_{min} = 1.82Å).

Water uptake experiment 2:

The same powder sample **P3**, as previously described in section 2.3.10 was used for the study after cutting open the end of the capillary tube. 1 hr X-ray powder patterns were recorded at set periods of time over a 42 day period (Table 9) in an analogous manner to study 1. The unit cell parameters of the obtained patterns (**W2.1** to **W2.8**) were determined using Pawley refinements. The unit cell parameters and final indices of fit are listed in Table 12. Extended fitting details are given for representative powder patterns **W2.4** and **W2.8** only. A stacked plot of the powder diffraction patterns is shown in Figure 20.

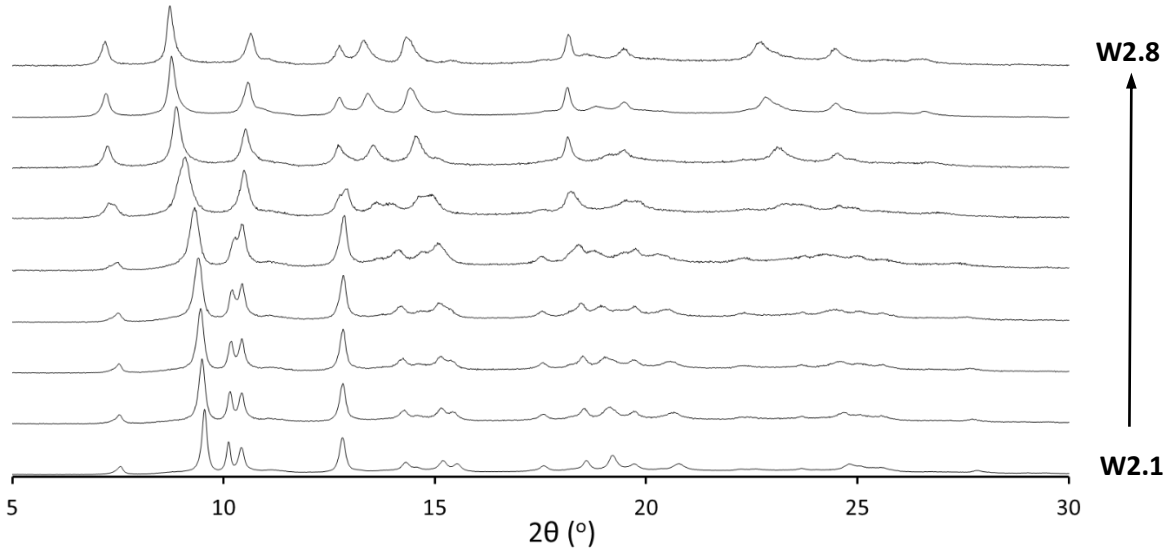

Figure 20 - Powder patterns of partially desolvated as-synthesised $(Me_2NH_2)[In(ABDC)_2]$ recorded at 30 min intervals while exposed to atmospheric water vapour (**W2.1 – W2.8**)

Table 12 - Refined unit cell parameters for water uptake experiment 1 (**P3**, **W2.1** to **W2.8**)

Code	Time	*a* (Å)	*b* (Å)	*c* (Å)	*V* (Å^3)	R_{wp}	$R_{wp'}$
P3	0	15.004(3)	21.764(6)	34.838(9)	11377(4)	6.817	14.491
W2.1	12hrs	15.008(4)	21.984(8)	34.71(1)	11451(6)	7.401	15.298
W2.2	24hrs	15.011(5)	22.12 (2)	34.63(2)	11499(9)	8.487	18.098
W2.3	2 days	14.992(5)	22.28 (1)	34.45(2)	11506(9)	7.877	16.542
W2.4	3 days	14.991(7)	22.61 (2)	34.29(3)	11624(14)	8.010	17.822
W2.5	6 days	15.08(4)	23.65 (4)	33.7(3)	11983(106)	8.400	17.698
W2.6	13 days	15.30(2)	24.87 (3)	32.82(5)	12493(28)	6.656	14.859
W2.7	19 days	15.344(9)	25.58(2)	32.33(2)	12687(13)	5.833	13.211
W2.8	42 days	15.40(1)	26.01(2)	31.94(3)	12799(20)	6.209	14.941

Representative fitting for water uptake experiment 2

W2.4: The unit cell was initially determined by analysis of the positions of the first few Bragg reflections and their known Miller indices. These unit cell parameters were used as a starting point for the Pawley refinement, employing 159 parameters (6 background, 1 zero error, 5 profile, 3 cell and 144 reflections), resulting in final indices of fit R_{wp} = 8.010, $R_{wp'}$ = 17.822. The final unit cell parameters were orthorhombic a = 14.991 (7) Å, b = 22.61 (2) Å, c = 34.29 (3) Å, V = 11624 (14) Å^3.

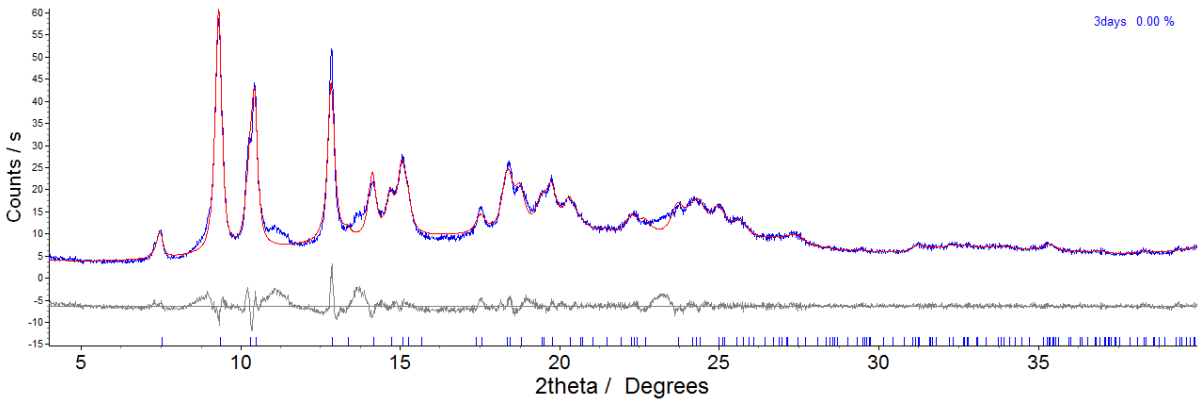

Figure 21 - Observed (blue) and calculated (red) profiles and difference plot [I_{obs}-I_{calc}] (grey) for the Pawley[17] refinement of **W2.4** (2θ range 4.0 – 40.0 °, d_{min} = 2.56Å).

W2.8: The unit cell was initially determined by analysis of the positions of the first few Bragg reflections and their known Miller indices. These unit cell parameters were used as a starting point for the Pawley refinement, employing 172 parameters (8 background, 1 zero error, 5 profile, 3 cell and 291 reflections), resulting in final indices of fit R_{wp} = 6.209, $R_{wp'}$ = 14.941. The final unit cell parameters were orthorhombic a = 15.40 (1) Å, b = 26.01 (2) Å, c = 31.94 (3) Å, V = 12799 (20) Å^3.

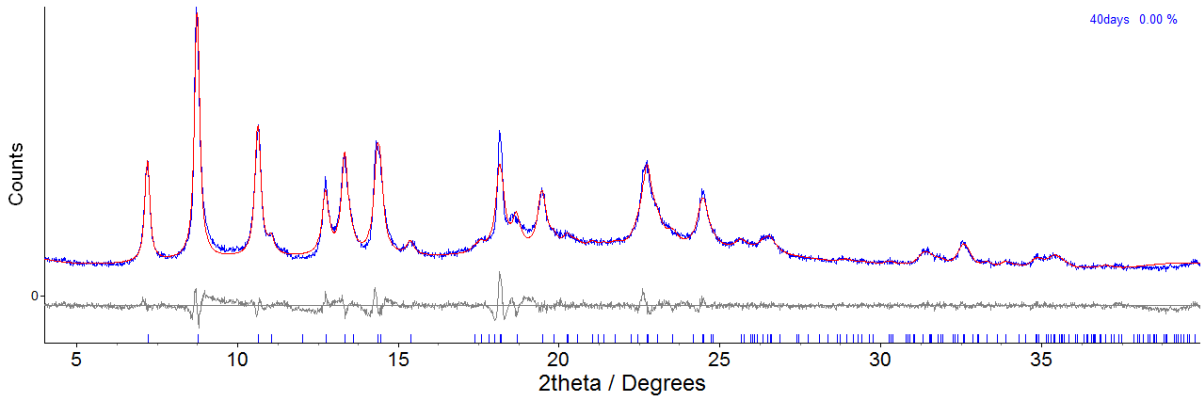

Figure 22 - Observed (blue) and calculated (red) profiles and difference plot [I_{obs}-I_{calc}] (grey) for the Pawley[17] refinement of **W2.8** (2θ range 4.0 – 40.0 °, d_{min} = 2.56Å).

2.3.12 Temperature dependant structural changes of as-synthesised $(Me_2NH_2)[In(ABDC)_2]$

Single Crystal diffraction

The crystal used for the variable temperature measurements was partially desolvated by *in situ* heating methods prior to cooling using the Cryostream device. The crystal was initially selected while immersed in the mother liquor and one face of the crystal was glued to a glass fibre while the crystal was still covered in a thin layer of residual solvent. Care was taken to avoid coating the entire crystal in adhesive. The crystal was rapidly transferred to the diffractometer and situated in the nitrogen stream of the Cryostream device at room temperature. The glue was left to dry for 15 mins before the *in situ* heating was carried out using the Cryostream device. A ramp rate of 4 °C/min was used to raise the temperature to 150 °C, which was held for 15 minutes before cooling at the same ramp rate. An intensity data collection was recorded under the nitrogen stream at 298 K, using the Cryostream to maintain the temperature (**H4.1**). A ramp rate of 4 °C/min was then used to lower the temperature of the cyrostream to 200 K (**H4.2**) and 100 K (**H4.3**), recording intensity data collections at each temperature after 5 minutes equilibration. The unit cell parameters were obtained by analysing reflections of I/σ > 10 from 4 sets of 10° omega scans with 0.5° slicing. Table 13 details the variable temperature study and the resulting cell parameters.

Table 13 - Unit cell values determined for crystallographic studies of temperature dependence on a partially desolvated as-synthesised MOF $(Me_2NH_2)[In(ABDC)_2]$

Temperature	Data set code	*a* (Å)	*b* (Å)	*c* (Å)	*V* (Å^3)
298 K	**H4.1**	14.924(8)	21.85(1)	34.82(1)	11355(8)
200 K	**H4.2**	14.874(8)	21.698(9)	34.91(1)	11266(7)
100 K	**H4.3**	14.85(1)	21.24(1)	35.15(1)	11087(9)

Powder Diffraction

A sample of as-synthesised $(Me_2NH_2)[In(ABDC)_2]$ was packed into a 0.7mm borosilicate capillary and placed inside a temperature controlled oven. The temperature was raised to 150 °C and held at this temperature for 4 hours. The capillary was subsequently removed from the oven and immediately flame sealed. A 1 hour data collection was recorded under the nitrogen stream at 298 K, using the Cryostream to maintain the temperature (**P4.1**). A ramp rate of 4 °C/min was then used to lower the temperature of the Cyrostream to 200 K (**P4.2**) and then 150 K (**P4.3**), recording 1 hour data collections at each temperature. The unit cell values determined from Pawley[17] refinements are displayed in Table 14. Stacked powder diffraction patterns are displayed in Figure 23 and representative fitting of **P4.2** is detailed below.

Table 14 - Unit cell values determined for crystallographic studies of temperature dependence on a powder sample of partially desolvated as-synthesised MOF $(Me_2NH_2)[In(ABDC)_2]$

Temperature	Data set code	*a* (Å)	*b* (Å)	*c* (Å)	*V* (Å^3)
298 K	**P4.1**	15.210(2)	23.660(4)	33.704(8)	12129(4)
200 K	**P4.2**	15.1292(9)	22.803(2)	34.216(4)	11804(2)
150 K	**P4.3**	15.102(1)	22.557(2)	34.357(4)	11704(2)

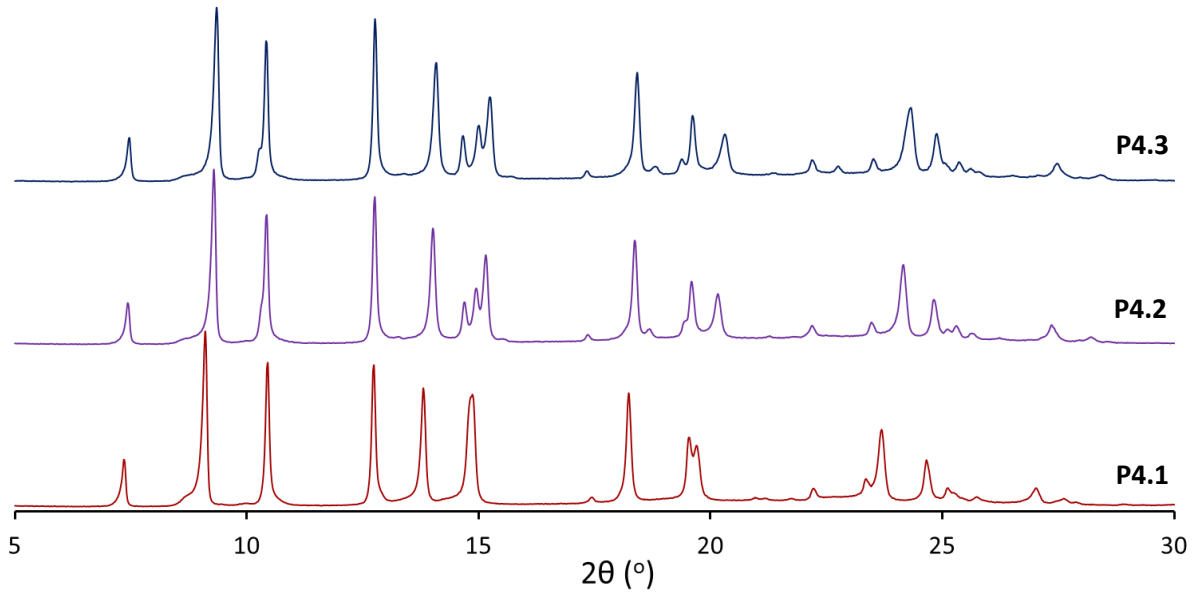

Figure 23 - Powder patterns of partially desolvated as-synthesised $(Me_2NH_2)[In(ABDC)_2]$ recorded at differing temperature using a Cryostream (**P4.1 – P4.3**)

P4.2: The unit cell was initially determined by analysis of the positions of the first few Bragg reflections and their known Miller indices. These unit cell parameters were used as a starting point for the single-phase Pawley refinement, employing 287 parameters (6 background, 1 zero error, 5 profile, 3 cell and 272 reflections), resulting in final indices of fit R_{wp} = 9.997, $R_{wp'}$ = 15.245. The final unit cell parameters were orthorhombic a = 15.1292 (9) Å, b = 22.803 (2) Å, c = 34.216 (1) Å, V = 11804 (2) Å^3.

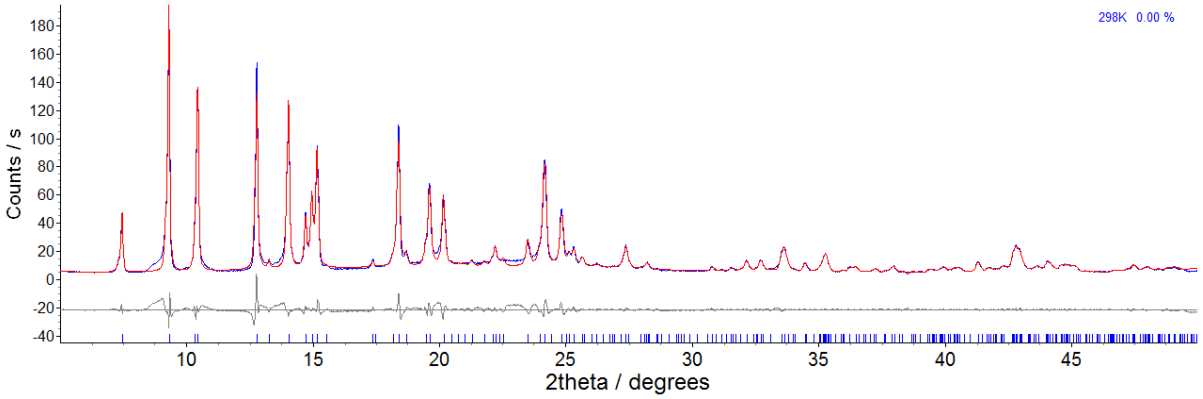

Figure 24 - Observed (blue) and calculated (red) profiles and difference plot [I_{obs}-I_{calc}] (grey) for the Pawley[17] refinement of **P4.2** (2θ range 4.0 – 50.0 °, d_{min} = 1.82Å).

2.4 Results and Discussion

2.4.1 Synthesis of $(Me_2NH_2)[In(ABDC)_2]$

The MOF synthesised using the procedure detailed in the experimental section produced brown octahedron-shaped crystals suitable for study by single crystal X-ray diffraction. To confirm the framework structure and the reproducibility of the synthetic method, three full diffraction data sets were collected using crystals from three different batches (**1-3**). The obtained crystal structures closely match the published structure,[1] but unlike the published structure a crystallographic model in which the aromatic ring was modelled as disordered over two orientations, with a refined 50:50 occupancy, was found to give the best fit to the experimental data. Figure 25 shows the ellipsoid plot for one of the crystal structures, illustrating the model with and without disorder, the secondary component in the disordered structure is shown in light blue. $Me_2NH_2^+$ counterions were able to be modelled inside the pore using crystallographic restraints, but no guest solvent molecules were able to be located. The cations were disordered and have been removed from images for clarity.

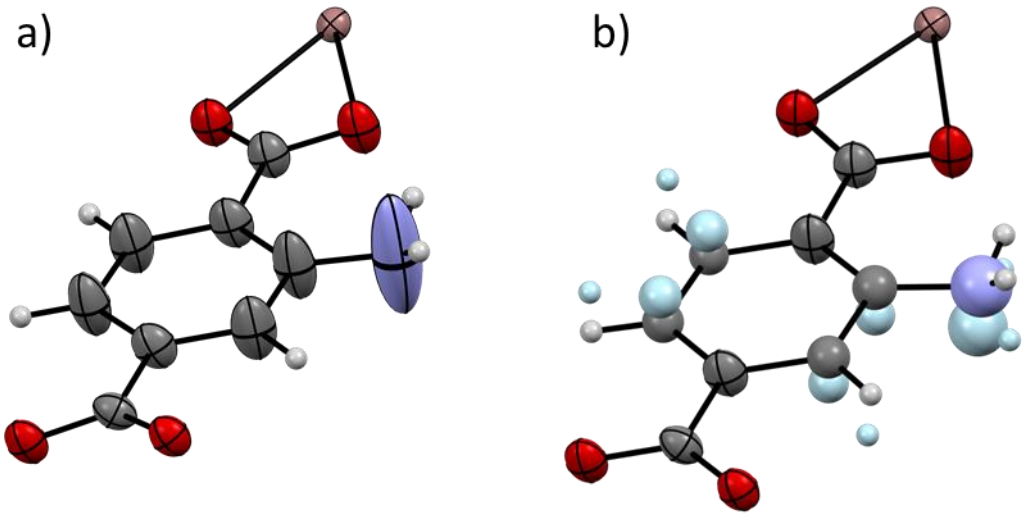

Figure 25 – Asymmetric unit of $(Me_2NH_2)[In(ABDC)_2]$ showing a) modelling without disorder, b) model with disorder of the ring and amine. Displacement ellipsoids are shown are the 50% probability level. In the primary component Indium atoms are in pink, carbon atoms in grey, oxygen atoms in red and nitrogen atoms in blue. In the second component of the disorder model all atoms are displayed in light blue.

The exact solvent content is currently unknown but can be estimated using several different methods; Least squares fitting of the elemental analysis suggests the framework contains 1.75 DMF molecules and 1.25 H_2O molecules per indium centre, digested NMR analysis suggests approximately 2 DMFs per indium but isn't able to quantify the number of water molecules, and analysis of the residual electron density in the pores of **1-3** by the routine SQUEEZE[8] gives an electron count ranging from 94 – 177 per formula unit, which could be associated with roughly 2 - 2.5 DMF molecules and 1.5 - 1.75 H_2O molecules.

Room temperature powder diffraction data were collected to check for phase purity (**P1**). The pattern indexed to a single phase and a Pawley refinement showed a good fit to a face centred orthorhombic cell of similar dimensions to those obtained from the single crystal measurements. A rigid model for the MOF, based on the single crystal structures, was used as a starting point for the Rietveld refinement, where the positions and orientations of the cation and solvent molecules (modelled as rigid bodies) were optimised by simulated annealing. The Rietveld[20] refinement also showed a good fit to the experimental data (Figure 5) and confirms the bulk structure is the same as that of the single crystals.

2.4.2 Crystal structure analysis

Amine interactions

In-depth analysis of the obtained crystal structures revealed an amine-amine hydrogen bonding interaction between the two interpenetrated frameworks. This has been emphasised in Figure 26 and is suspected to add stability to the two-fold interpenetrated structure. The interaction shows a H···N distance of 2.61 Å, a C-N-N angle 144.9 ˚ and a N-H-N angle of 120 ˚ (Hydrogen lengths were normalised to neutron values).

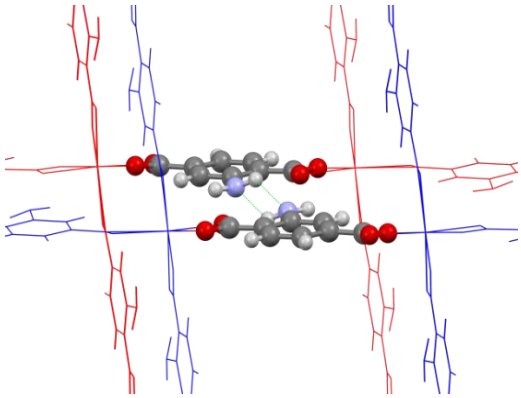

Figure 26 - The amine-amine hydrogen bonding interactions between interpenetrated frameworks

Evidence for this hydrogen bonding interaction playing an important role in defining the final framework topology is provided by the absence of disorder of the amine site around the aromatic ring, and the fact that an isostructural MOF is not obtained when terephthalic acid is used in place of 2-aminoterephthalic acid in the synthesis. Following the same experimental procedure using the unsubstituted terephthalic acid leads instead to the formation of the known framework QMOF2 [InH(BDC)$_2$]. This framework contains a secondary building unit almost identical to (Me_2NH_2)[In(ABDC)$_2$], but a different arrangement of the interpenetrated chains and a quartz like topology.[22] This phase was identified by powder diffraction analysis (**PQ**), which also confirms the phase purity.

Differences in structure between different crystals

A more detailed comparison of the 3 obtained as-synthesised crystal structures (**1-3**) showed a significant variation in the unit cell parameters. The unit cell values for the three crystal structures are recorded in Table 15 and display up to a 0.8 Å difference in the *b*-axis and 0.6 Å change in the *c*-axis, while little change is observed in the *a*-axis. These changes are far beyond any experimental error or differences that would be expected for crystals recorded at the same temperature. The framework structures retain the same network and connectivity but the changes result in slight variations in the dimensions of the materials channels, which lie parallel to the *b*- and *c*-axes. The desolvation studies presented in 2.4.3 shed further light on this phenomenon.

Table 15 - Unit cell parameters of crystal structure **1-3** (as-synthesised In MOF) (Me_2NH_2)[In(ABDC)$_2$]

Crystal No.	*a* (Å)	*b* (Å)	*c* (Å)	*V* (Å^3)
1	15.3069(5)	26.9467(8)	31.284 (1)	12903.7(3)
2	15.2451(4)	26.7998(8)	31.3225(8)	12797.3(6)
3	15.155(3)	26.139(6)	31.908(7)	12640(5)

2.4.3 Desolvation Studies

Overview of Experiments

To understand the behaviour of the framework during solvent removal, 7 crystal structures (**4-10**) were obtained by drying single crystals of the framework in air at different temperatures. The temperatures (RT, 100 °C and 150 °C) were chosen based on the thermogravimetric analysis which displayed a large mass loss associated with solvent removal between 100 °C and 175 °C. The TGA analysis also showed two further steps consistent with loss of Me_2NH from cation loss, which should lead to framework protonation, at 250 °C, and decomposition of the organic components of the framework at 400 °C. The three different temperatures were designed to probe various levels of partial desolvation, not just full solvent removal. The crystals retained most of their crystallinity throughout the treatments, allowing accurate characterisation by single crystal X-ray diffraction. Attempts to heat crystals for longer or to higher temperatures resulted in a loss of crystallinity. The treatment conditions for crystals **4-10**, the effect on the unit cell volumes, and the residual electron count per indium centre from SQUEEZE[8] analysis of the diffraction data are displayed in Table 16.

Table 16 - Treatment methods used in ex situ desolvation studies of single crystal $(Me_2NH_2)[In(ABDC)_2]$

Crystal No.	Treatment Method	Unit Cell Volume (Å^3)	No of solvent e$^-$ per Indium
4	Dried in Air 2 hours	11870.1(9)	92
5	Dried in Air 14hrs	12284.9(6)	93
6	Heated to 100 °C for 10 mins	11979(7)	75
7	Heated to 150 °C for 5 mins	11361.9(5)	65
8	Heated to 150 °C for 5 mins	11311(4)	47
9	Heated to 150 °C for 15 mins	10961.9(10)	44
10	Heated to 150 °C for 15 mins, left in air for 2 days	12564(2)	81

Extent of desolvation

The extent of solvent removal in the various crystal treatments (**4-9**) can be estimated using the electron counts in Table 16, however the reliability of the values will be highly dependent on the quality of the crystallographic model and the diffraction data, which was not always very high, and therefore should only be taken as a guide. The electron counts show that air treated crystals display similar values to that seen from the as-synthesised framework but the heated crystals show a reasonable but not complete solvent loss. Solution-phase ^{1}H NMR spectroscopy and solid-state IR spectroscopy were also used to characterise the extent of desolvation in crystal **9** (the most desolvated crystal). The NMR analysis (Figure 10) suggested 0.55 DMF molecules per indium remaining in the pore, a significant reduction to the 2 DMF molecules in the as-synthesised framework, and the solid-state IR (Figure 12) showed a substantial reduction of the DMF carbonyl peak at 1657 cm^{-1}.

Effect of solvent removal on the crystallographic dimensions

Crystals **4-10** display a wide range of unit cell parameters, different to each other, and to the as-synthesised structures **1-3**. The largest changes in comparison to the as-synthesised sample were observed for crystal **9**, which showed a contraction of 6 Å in the *b*-axis (reduction to 78 % of its original length) and a lengthening of 4 Å in the *c*-axis (to 113 % of its original length). This results in a unit cell volume change of approximately 2000 $Å^3$, (a 15 % change). In contrast, however, the *a*-axis showed only much smaller changes (0.4 Å). Using crystal **1** as a reference the normalised changes to each of the crystallographic axes have been plotted in Figure 27. The largest differences being exhibited by the most desolvated crystal implies the changes are at least partially related to solvent loss.

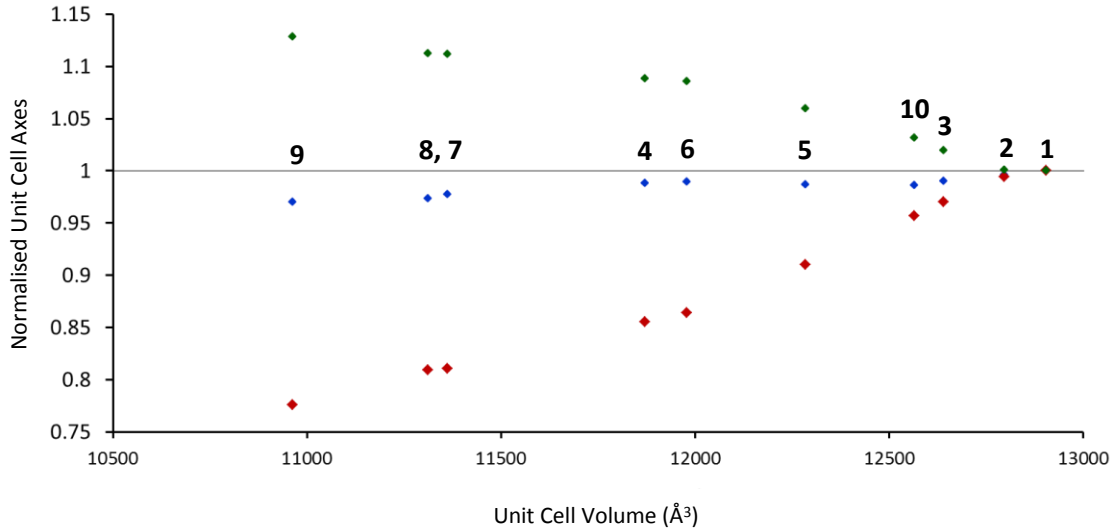

Figure 27 - Normalised unit cell axis lengths in comparison to the unit cell volume for single crystal desolvation studies of as-synthesised $(Me_2NH_2)[In(ABDC)_2]$. Blue Diamonds; *a*-axis, Red diamonds; *b*-axis, Green Diamonds; *c*-axis.

Changes to the pore structure

The changes to the unit cell dimensions are a reflection of the significant structural changes that are occurring in the framework. The *b*- and *c*-axes directly relate to the cross-section dimensions of the framework channels, which undergo a shape change during the desolvation. The SQUEEZE[8] routine suggests this corresponds to a 31% reduction in the solvent accessible. This change to the porosity is demonstrated in Figure 28 by looking at the structure of crystals **1** and **9**.

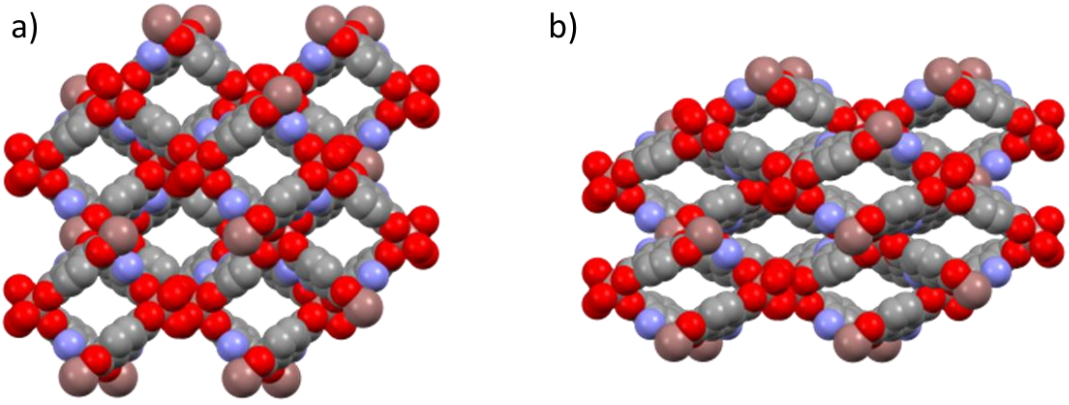

Figure 28 - Spacefill view down the *a*-axis of a) **1** and b) **9**

When viewed down the *a*-axis, this structural change initially appears to be a smaller scale analogous motion to the well-known flexible MOF MIL-53(Cr) [Cr(OH)(BDC)], which displays a 2D "wine-rack" breathing mode. The flexibility in MIL-53 results in its lozenge-shaped channels narrowing in similar manner to crystal **9**, most notably during transitions from its high temperature (empty) to low temperature (hydrated) forms.[23] The change in MIL-53(Cr) is significantly larger than in crystal **9**, resulting in a 32% change in volume, [23] and an associated larger reduction in the channel dimensions. MIL-53 however does not contain a counter-ion in the pores. A representation of the change in structure during breathing of MIL-53 is shown in Figure 29.

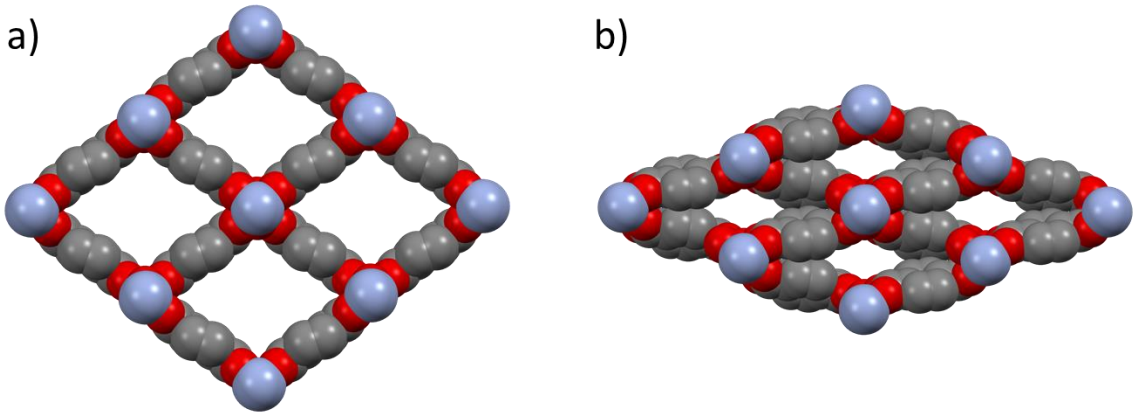

Figure 29 - Spacefill representations of the difference in structure exhibited by MIL-53 when a) empty (open-pore) and b) monohydrated (closed-pore). Guest water molecules have been removed for clarity from the hydrated version

Although the overall effect on the pore shape between MIL-53 and $(Me_2NH_2)[In(ABDC)_2]$ seem very similar, the mechanism behind the flexibility is different, due to the differences in the structures of the two materials. MIL-53 exhibits an infinite array of metal ions bridged by carboxylates and hydroxyl groups in one dimension, and connections between the metal ion chains via the dicarboxylate ligands in the other 2 dimensions. This makes the framework very much like a wine rack where no movement is possible along the direction parallel to the metal ion array (the framework channels). Figure 30 demonstrates the building unit of structure.

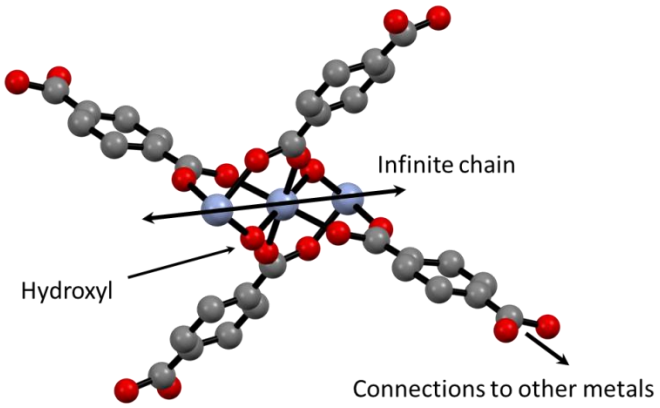

Figure 30 - Ball and stick representation of the building unit in MIL-53(Cr)

The breathing of MIL-53 is therefore caused by the oxygens on benzenedicarboxylate ligands acting as a knee-cap and moving the ligand out of the plane of the connection between the two metal ion arrays. This is displayed looking at the as-synthesised and monohydrated (closed-pore) versions of MIL-53 in Figure 31.

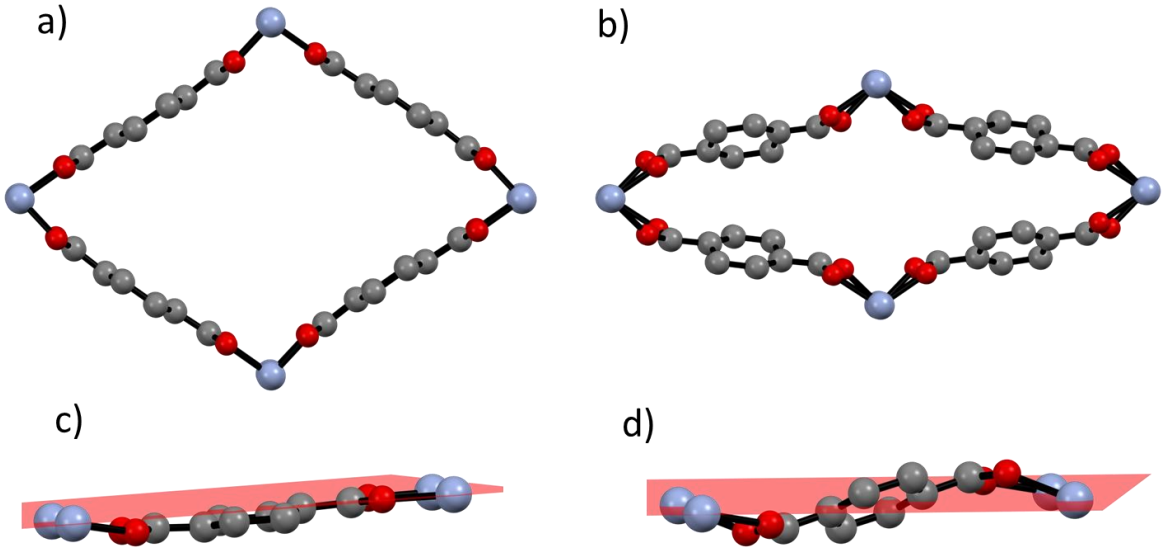

Figure 31 - Changes observed to the ligand environment in the a) as-synthesised (open-pore) and b) hydrated (closed-pore) MIL-53(Cr). The plane defining the connection between the metal arrays for the two forms is shown in c) and d) respectively

$(Me_2NH_2)[In(ABDC)_2]$ does not have the same wine-rack network connectivity as MIL-53, but only has channels which are similarly lozenge-shaped when being viewed down the *a*-axis (*i.e.* down its channels). The framework instead has a diamondoid network, with connections between indium ions occurring in all three dimensions, via chelating aminobenzenedicarboxylate ligands. This gives the structure more freedom, allowing larger distortions to the geometry around the metal centre. The structural changes therefore occur predominantly due to a twisting of the flattened tetrahedral coordination environment, combined with only a small knee-cap effect. This is demonstrated in Figure 32. The degree of the knee-cap effect can be measured using the metal (or metal…metal centroid in the case of MIL-53) to O…O centroid to carboxyl carbon angle. In MIL-53 the open to closed transition changes this angle from 180 ° to 164 °, and in $(Me_2NH_2)[In(ABDC)_2]$ the change is between is 176 ° to 168 ° (**1** and **9**).

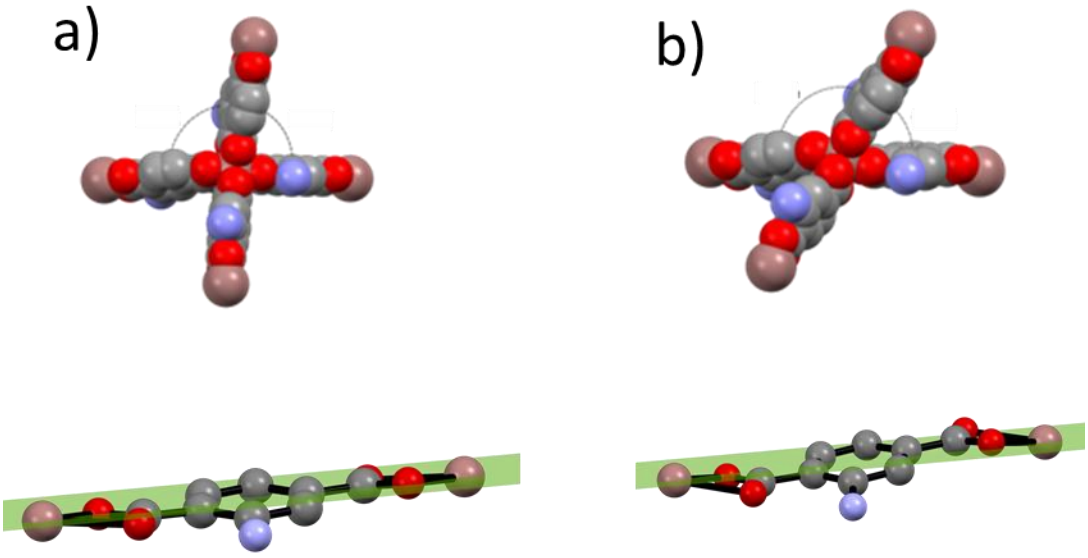

Figure 32 - Structural effects occurring to $(Me_2NH_2)[In(ABDC)_2]$ during desolvation a) Crystal **1**, b) Crystal **9**

Monitoring the extent of breathing

The breathing effect of $(Me_2NH_2)[In(ABDC)_2]$, despite the differences from the wine-rack structure of MIL-53, is still predominantly two-dimensional with the helical chains running parallel to the *a*-axis mostly remaining unchanged. The changes in the *b*- and *c*-axes can therefore be used to quantify the extent of the breathing. Figure 33 plots the *b*-axis against the *c*-axis, showing a high linear correlation between the two axes. A representation of the pore shape, determined crystallographically, is shown above each point to demonstrate the structural changes. The as-

synthesised crystals (**1-3**) are included in the plot showing the observed variation in them also lies along the same trend line.

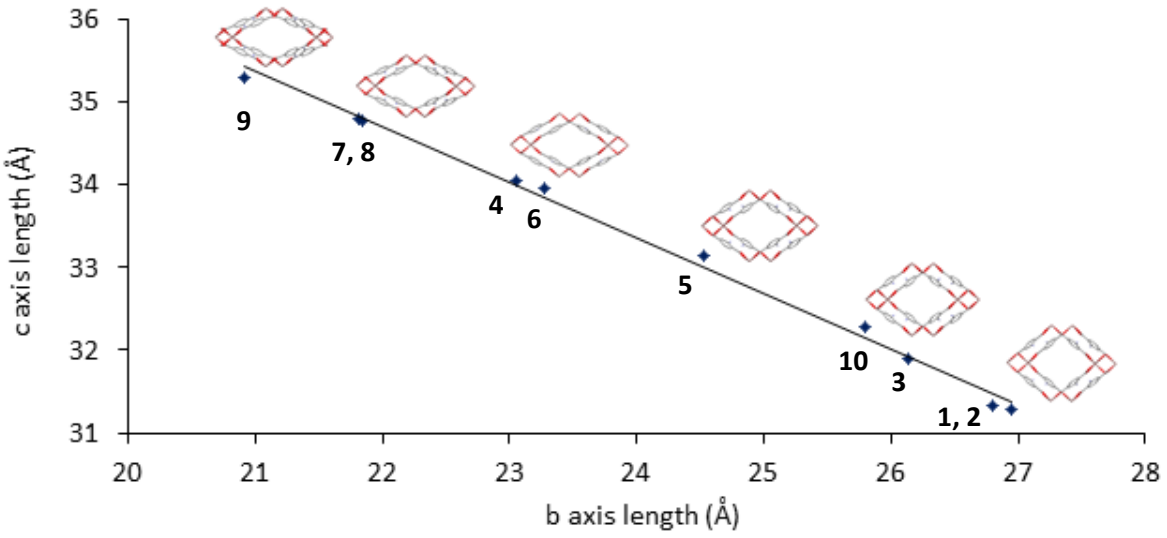

Figure 33 - Changes to the *b*- and *c*-axis lengths of as-synthesised $(Me_2NH_2)[In(ABDC)_2]$ determined by single crystal diffraction during various stages of solvent removal (**1-10**). Above each point a representation of the changing pore geometry is displayed from each crystal structure; modelled framework disorder has been removed for clarity.

The crystal structures mostly follow a logical order, the as-synthesised crystals **1** & **2**, correspond to an open pore structure with maximum guest loading, crystal **3** shows a slightly closed structure due to small variations in the solvent content, crystals **5** displays a more closed structure, most likely due to a change in the relative ratio of DMF and H_2O on exposure to air, and crystals **6-9** display higher levels of closing due to the heating procedures. Heating to higher temperatures or for increased time also resulted in larger changes. Crystal **10** followed the same heating procedure as **9** but was subsequently left in the air for two days, and shows an open structure, implying a return towards the as-synthesised framework over time. This is coupled with a larger number of residual electrons and is anticipated to be associated with water uptake from the atmosphere, consistent with the experiments described in Section 2.3.11 and discussed Section 2.4.5. The results in general suggest that the pore size and shape is roughly related to the number or type of guest molecules remaining in the MOF. Crystal **4** appears to be an anomaly, showing a reasonably closed structure, after only air drying. Structures **7** and **8** following the same treatment show a very similar overall breathing, however display reasonably different electron counts. This may be due to quality of data in crystal **8** which was substantially lower, making the residual electron count less reliable.

The large number of unique crystal structures shown in Figure 33, is more than would be expected to be low energy structural intermediates in a normal open-pore to closed-pore phase transition.

MIL-53(Cr) for example shows only an open and a closed phase, MIL-53(Fe) shows 4 phases, and CoBDP (BDP = 1,4-benzenedipyrazolate), which exhibits one of the most complicated multi-step breathing modes, shows only 5 phases.[23–26] This suggests that the MOF's flexibility might instead be occurring through a continuous process, with the degree of closing only being determined by the amount of solvent still contained in the pore. Assuming the behaviour of the framework structure continues to follow the same motion, the fully desolvated framework structure is expected to lie even further along the same trend line and be the most closed form of the MOF.

2.4.4 Bulk-phase characterisation of the breathing effect

The breathing motion of the as-synthesised framework during solvent removal was confirmed as a bulk property of the material by monitoring the structural changes using X-ray powder diffraction. Two heating experiments were conducted (**P2** and **P3**) and the unit cell values of the resulting structures were analysed by Pawley refinements (Figure 14 and Figure 15). The unit cell values lie along the linear trend line obtained from the single crystal data; the as-synthesised material (**P1**) closely resembles the fully open-pore, consistent with full solvation, the sample heated in an open container under inert atmosphere (**P3**) displays a highly closed pore and the sample heated in the capillary (**P2**) adopts a structure midway between these two extremes. This can be rationalised, as the removal of solvent within a capillary tube is substantially harder than in an open container.

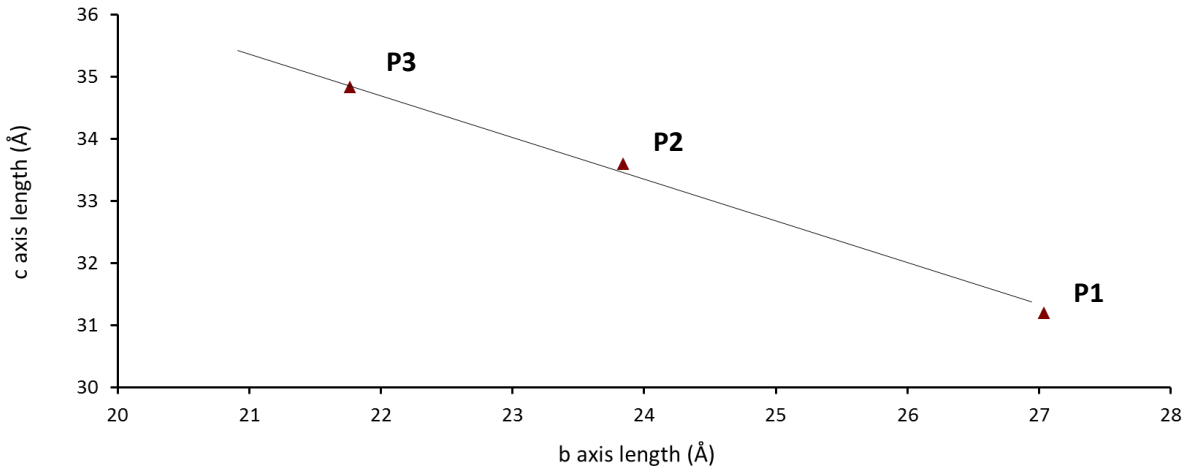

Figure 34 - Unit cell variations for *ex situ* heated powders of as-synthesised samples of $(Me_2NH_2)[In(ABDC)_2]$, obtained from Pawley refinements of X-ray powder diffraction data. The trendline is calculated using unit cell parameters of *ex situ* heated single crystals.

2.4.5 Atmospheric water uptake

Crystal **10** suggested the possibility of water uptake from a partially desolvated structure. Attempts to observe these effects using desolvated powder samples open to air resulted in a rapidly changing powder diffraction pattern over the space of only 5 mins, making it experimentally difficult to monitor the water uptake process on a suitable timescale. To overcome this difficulty the experiments described in section 2.3.11 were designed. The exposure of the powder to air via the small aperture of the capillary slowed down the facile water adsorption allowing it to be successfully monitored over time. The structural effects were determined by Pawley refinements of the powder patterns (**W1.1 – W1.24**) and showed the continuous evolution of the structure towards an open pore form. The unit cell values from the experiment lie close to the single crystal trend, and are displayed in Figure 35. The green triangle refers to the minor open-pore phase also fitted in the refinements.

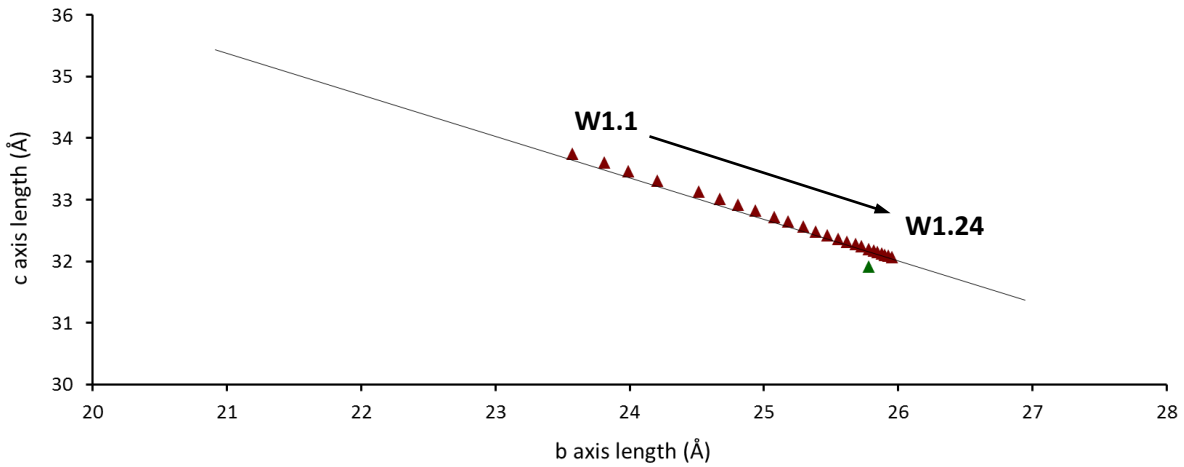

Figure 35 - *b*- and *c*-axis values from successive Pawley refinements of powder patterns recorded every 30 mins during atmospheric water uptake experiment 1. Red triangles, major phase; green triangle, minor phase present after heating. The trend line is calculated using unit cell parameters of *ex situ* heated single crystals (**1-10**).

The rate of change in the unit cell dimensions was observed to decrease over time as the pore approached an open structure and became more saturated. The changes in the *b*- and *c*-axes over time are shown Figure 36. The slow movement of powder diffraction peaks without significant peak broadening suggests a consistent pore opening (of the major phase) between all crystallites sampled by the X-ray beam during the experiment. This implies a fast equilibration between the crystallites, which avoids the broadening of the peaks that might expected due to a statistical distribution of phases (and pore dimensions) in uneven water adsorption.

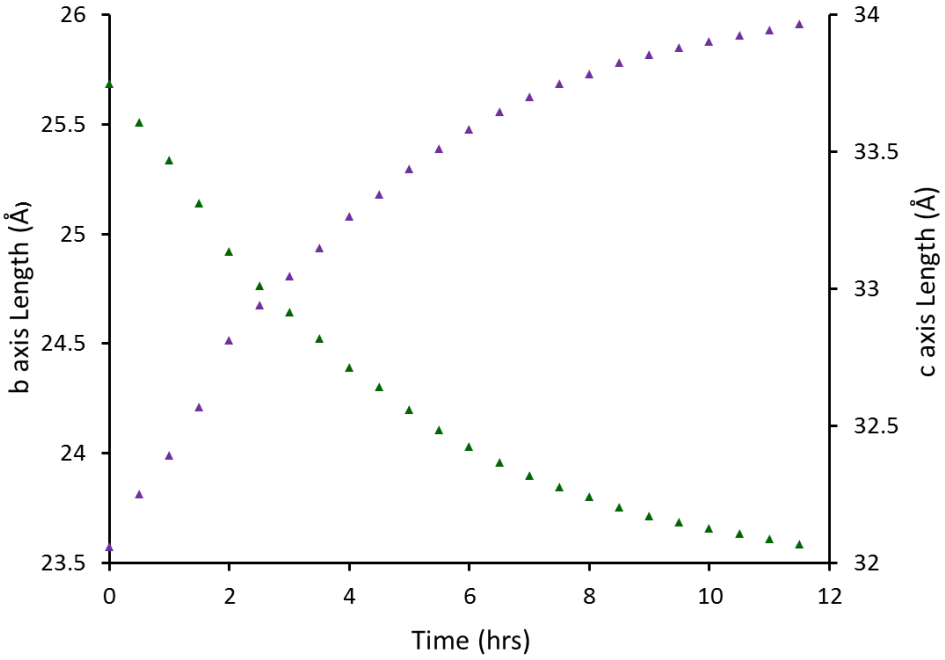

Figure 36 - *b*- and *c*-axis values *vs* time from successive Pawley refinements of powder patterns from *in situ* heating experiment 1. Purple triangles, *b*-axis; green triangles *c*-axis.

Atmospheric water vapour uptake was also studied starting from powder **P3**, which showed a position significantly further along the single crystal trend line, implying a higher desolvation and a more closed structure than the starting point of the first water uptake experiment, **W1.1**. The details of the experiment are provided in Table 12 and the changes along the trend line defined by the single crystal experiments are shown in Figure 37. The powder patterns (**W2.1** – **W2.8**) show a similar reopening of the pores, but on a much slower time scale. This suggests significantly slower kinetics occurring in the narrower pore. Unfortunately the two different water uptake experiments were carried out in capillaries of different internal diameters so no strong conclusions can be drawn from the change in time scale.

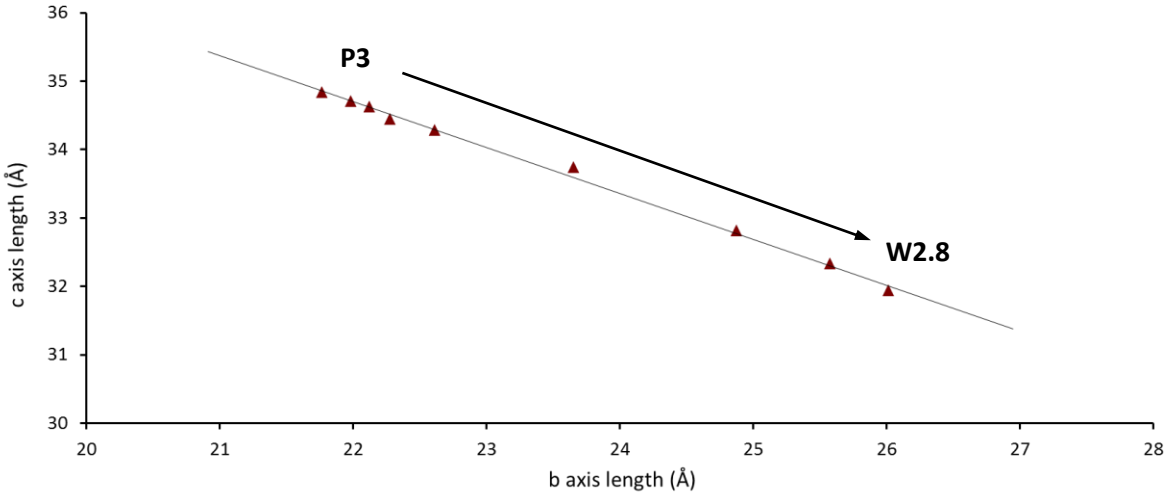

Figure 37 - b and c axis values from successive Pawley refinements of powder patterns recorded every 30mins during atmospheric water uptake experiment 1. Red triangles Major Phase, Green triangle minor phase present after heating. The trend line is calculated using unit cell parameters of *ex situ* heated single crystals (**1-10**).

Overall both water uptake experiments show a high reversibility to the breathing effect, and that the process occurs through a continuous structural evolution rather than through defined phase transitions, which are common among the majority of flexible MOFs.

2.4.6 Crystallographic studies of desolvation using *in situ* heating methods

To more accurately assess the desolvation of the framework, without the complications arising due to absorption of atmospheric water, the MOF was studied crystallographically by *in situ* heating methods. The details of the experiments can be found in Section 2.3.8 and Table 7. These experiments allowed a single crystal to be chosen with minimal exposure to air and heated while surrounded by an inert nitrogen atmosphere. Three heating experiments were carried out and the results are displayed Figure 38 compared to the trend line from crystals **1-10**. Heating studies 1, 2 and 3 are shown in red, blue and green respectively. The filled triangles in Figure 38 refer to points where full structural solutions were obtained (**H1.6** and **H2.2**).

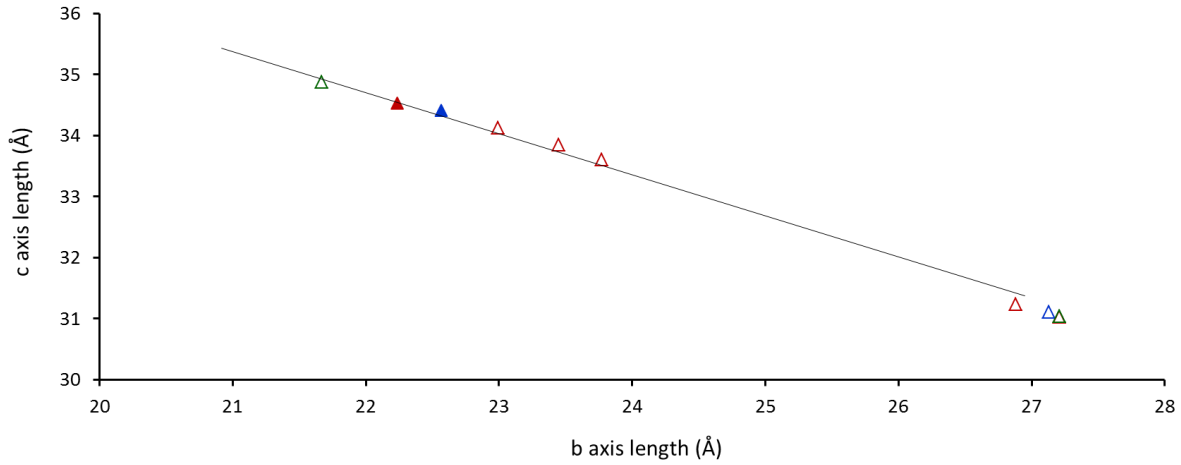

Figure 38 - *b*- and *c*-axis values for *in situ* heating experiment 1 (red), 2 (blue) and 3 (green). Filled traingles refer to full data sets (with structure determination); open triangles refer to unit cell determinations only. The trend line is calculated using unit cell parameters of *ex situ* heated single crystals (**1-10**).

The data points lie close to the trend line and provide more evidence of the wide range of different pore openings available to the framework. All the studies showed a fully open-pore structure while under the nitrogen atmosphere at the start of the experiment, confirming that the closing seen for **4** and **5** was due to the exposure of crystals to water in the air and not the removal from solvent. Various heat treatments then caused differing closed forms of the MOF, with heating study 1 displaying a progressive closing after heating to increasing temperatures, and heating studies 2 and 3 showing highly closed structures after heating directly to 150 °C. SQUEEZE analysis of the full crystal structures at the end of the studies shows substantially reduced electron counts to the as-synthesised framework, suggesting reasonable solvent loss. These experiments therefore confirm that the flexibility is occurring in a single-crystal-to-single-crystal manner and as a direct result of the heating. Visual images of the crystal recorded during heating experiment 3 (**H3.1** and **H3.2**) show that the flexibility of the framework also directly affects the morphology of the single crystal (Figure 39). The change in shape appears to be consistent with the changes in the crystal structure, although face indexing was not carried to confirm which dimensions had changed.

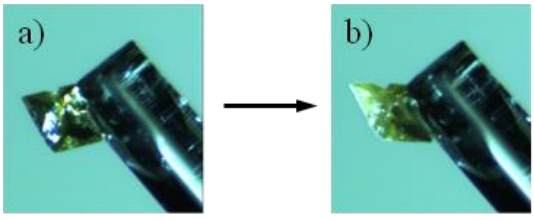

Figure 39 - Observed changes to the morphology of a single crystal during *in situ* heating experiment 3. a) **H3.1** and b) **H3.2**

The data above were all recorded at room temperature to remove the effects of temperature-dependent structural changes, which were also found to lead to distortions along the known breathing trend line. This can be seen in Figure 40 showing the same partially desolvated crystal at 298K (**H4.1**), 200K (**H4.2**) and 100K (**H4.3**), further details are provided in section 2.3.12.

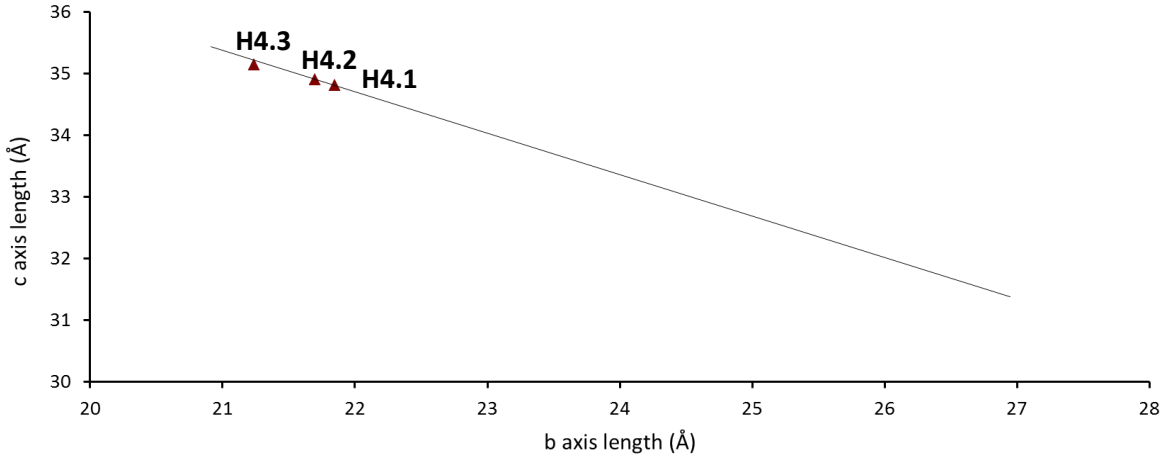

Figure 40 – *b*- and *c*-axis values for variable temperature experiment **H4**. All data is recorded on the same crystal, while at 298 K (**H4.1**), 200 K (**H4.2**) and 100 K (**H4.3**). The trend line is calculated using unit cell parameters of *ex situ* heated single crystals (**1-10**).

2.5 Conclusions

The desolvation of $(Me_2NH_2)[In(ABDC)_2]$ using both *in situ* and *ex situ* heating methods on both single crystal and powder samples has revealed a large continuous dynamic motion associated with the removal of solvent from the material. This effect is reversible upon exposure to water vapour, with the uptake being very facile at standard humidity values in the UK. The change in the pore shape mimics that of the well-known flexible MOF MIL-53, although as the two frameworks have different network topologies the breathing effect occurs through different molecular motions.

The continuous flexibility displayed in $(Me_2NH_2)[In(ABDC)_2]$ differs from the majority of flexible frameworks, which show defined phase transitions between open and closed structures during loss of their guest molecules, often involving a change in symmetry.[27–33] These flexible MOFs can display a continuum of framework structures based on induced fitting of differently interacting guests, but are often limited to displaying one phase while containing one guest.[34–36] The behaviour of the $(Me_2NH_2)[In(ABDC)_2]$ is therefore more similar to the MOF MIL-88, which is the prototypical MOF reported to display a continuous swelling mechanism.[37] MIL-88 ($Fe^{III}_3O(CH_3OH)_3\{O_2C\text{-}C_2H_2\text{-}CO_2\}\{O_2C\text{-}CH_3\}$) demonstrates a similar continuous structural evolution upon loss and uptake of water but is not so amenable to crystallographic characterisation and requires the aid of computational analysis for structure determination.[38] The work surrounding MIL-88 however is the only example of this behaviour within the literature. $(Me_2NH_2)[In(ABDC)_2]$ displays a significantly smaller scale flexibility than MIL-88, MIL-88D showing a huge volume increase of 170 %,[37] but provides a unique example of a continuous effect that can be accurately characterised using single crystal diffraction methods, offering detailed structural insight.

2.6 References

1 B. Yuan, D. Ma, X. Wang, Z. Li, Y. Li, H. Liu, and D. He, *Chem. Commun.*, 2012, 48, 1135–1137.

2 M. Eddaoudi, J. Kim, N. Rosi, D. Vodak, J. Wachter, M. O'Keeffe, and O. M. Yaghi, *Science*, 2002, 295, 469–472.

3 T. Ahnfeldt, N. Guillou, D. Gunzelmann, I. Margiolaki, T. Loiseau, G. Férey, J. Senker, and N. Stock, *Angew. Chem. Int. Ed.*, 2009, 48, 5163–5166.

4 S. J. Garibay, Z. Wang, K. K. Tanabe, and S. M. Cohen, *Inorg. Chem.*, 2009, 48, 7341–7249.

5 J. P. S. Mowat, S. R. Miller, J. M. Griffin, V. R. Seymour, S. E. Ashbrook, S. P. Thompson, D. Fairen-Jimenez, A.-M. Banu, T. Düren, and P. A. Wright, *Inorg. Chem.*, 2011, 50, 10844–10858.

6 H. Reinsch, M. Feyand, T. Ahnfeldt, and N. Stock, *Dalton. Trans.*, 2012, 41, 4164-4171.

7 R. Haldar, S. K. Reddy, V. M. Suresh, S. Mohapatra, S. Balasubramanian, and T. K. Maji, *Chem. Eur. J.*, 2014, 20, 4347–4356.

8 A. L. Spek, *Acta Crystallogr. C*, 2015, 71, 9–18.

9 A. L. Spek, *Acta Crystallogr. D.*, 2009, 65, 148–155.

10 SMART APEX II, *Bruker AXS, Madison, Wisconsin, USA*.

11 R. H. Blessing, *Acta Crystallogr. A*, 1995, 51, 33–38.

12 L. Krause, R. Herbst-Irmer, G. M. Sheldrick, and D. Stalke, *J. Appl. Crystallogr.*, 2015, 48, 3–10.

13 O. V. Dolomanov, L. J. Bourhis, R. J. Gildea, J. a. K. Howard, and H. Puschmann, *J. Appl. Crys.*, 2009, 42, 339–341.

14 G. M. Sheldrick, *Acta Crystallogr. A.*, 2008, 64, 112–22.

15 S. P. Thompson, J. E. Parker, J. Potter, T. P. Hill, A. Birt, T. M. Cobb, F. Yuan, and C. C. Tang, *Rev. Sci. Instrum.*, 2009, 80, 075107.

16 S. P. Thompson, J. E. Parker, J. Marchal, J. Potter, A. Birt, F. Yuan, R. D. Fearn, A. R. Lennie, S. R. Street, and C. C. Tang, *J. Synchrotron Radiat.*, 2011, 18, 637–648.

17 G. S. Pawley, *J. Appl. Cryst.*, 1981, 14, 357–361.

18 H. M. Rietveld, *Acta Cryst.*, 1966, 20, 508–513.

19 H. M. Rietveld, *Acta Cryst.*, 1967, 22, 151–152.

20 H. M. Rietveld, *J. Appl. Cryst.*, 1969, 2, 65–71.

21 A. A. Coelho, *TOPAS Academic. Version 4.1, 2007, see http//www.topas-academic.net*.

22 J. Sun, L. Weng, Y. Zhou, J. Chen, Z. Chen, Z. Liu, and D. Zhao, *Angew. Chem. Int. Ed.*, 2002, 41, 4471–4473.

23 C. Serre, F. Millange, C. Thouvenot, M. Noguès, G. Marsolier, D. Louër, and G. Férey, *J. Am. Chem. Soc.*, 2002, 124, 13519–13526.

24 F. Millange, N. Guillou, R. I. Walton, J.-M. Grenèche, I. Margiolaki, and G. Férey, *Chem. Commun.*, 2008, 4732-4734.

25 P. L. Llewellyn, P. Horcajada, G. Maurin, T. Devic, N. Rosenbach, S. Bourrelly, C. Serre, D. Vincent, S. Loera-Serna, Y. Filinchuk, and G. Férey, *J. Am. Chem. Soc.*, 2009, 131, 13002–13008.

26 F. Salles, G. Maurin, C. Serre, P. L. Llewellyn, C. Knöfel, H. J. Choi, Y. Filinchuk, L. Oliviero, A. Vimont, J. R. Long, and G. Férey, *J. Am. Chem. Soc.*, 2010, 132, 13782–13788.

27 R. Grünker, I. Senkovska, R. Biedermann, N. Klein, M. R. Lohe, P. Müller, and S. Kaskel, *Chem. Commun.*, 2011, 47, 490–492.

28 Y. Liu, Y.-P. Chen, T.-F. Liu, A. a. Yakovenko, A. M. Raiff, and H.-C. Zhou, *CrystEngComm*, 2013, 15, 9688-9693.

29 A. Demessence and J. R. Long, *Chem. Eur. J.*, 2010, 16, 5902–5908.

30 D. N. Dybtsev, H. Chun, and K. Kim, *Angew. Chem. Int. Ed.*, 2004, 43, 5033–5036.

31 A. Aijaz, P. Lama, and P. K. Bharadwaj, *Eur. J. Inorg. Chem.*, 2010, 2010, 3829–3834.

32 N. Klein, C. Herzog, M. Sabo, I. Senkovska, J. Getzschmann, S. Paasch, M. R. Lohe, E. Brunner, and S. Kaskel, *Phys. Chem. Chem. Phys.*, 2010, 12, 11778-11784.

33 Y. Sakata, S. Furukawa, M. Kondo, K. Hirai, N. Horike, Y. Takashima, H. Uehara, N. Louvain, M. Meilikhov, T. Tsuruoka, S. Isoda, W. Kosaka, O. Sakata, and S. Kitagawa, *Science (80-.).*, 2013, 339, 193–196.

34 F. Millange, C. Serre, N. Guillou, G. Férey, and R. I. Walton, *Angew. Chem. Int. Ed.*, 2008, 47, 4100–4105.

35 Y.-S. Wei, K.-J. Chen, P.-Q. Liao, B.-Y. Zhu, R.-B. Lin, H.-L. Zhou, B.-Y. Wang, W. Xue, J.-P. Zhang, and X.-M. Chen, *Chem. Sci.*, 2013, 4, 1539-1546.

36 Y.-X. Tan, F. Wang, Y. Kang, and J. Zhang, *Chem. Commun.*, 2011, 47, 770–772.

37 C. Serre, C. Mellot-Draznieks, S. Surble, N. Audebrand, Y. Filinchuk, and G. Ferey, *Science.*, 2007, 315, 1828–1831.

38 C. Mellot-Draznieks, C. Serre, S. Surblé, N. Audebrand, and G. Férey, *J. Am. Chem. Soc.*, 2005, 127, 16273–16278.